FOI-R--0315--SE
December 2001
ISSN 1650-1942

Scientific Report

Fredrik Kullander

Code Division Multiplexing in Networks of Interferometric Optical Fiber Sensors

Sensor Technology
SE-581 11 Linköping

SWEDISH DEFENCE RESEARCH AGENCY
Sensor Technology
P.O.Box 1165
SE-581 11 Linköping

FOI-R--0315--SE
December 2001
ISSN 1650-1942
Scientific report

Fredrik Kullander

Code Division Multiplexing in Networks of Interferometric Optical Fiber Sensors

Issuing organization	Report number, ISRN	Report type
FOI-Swedish Defence Research Agency Division of Sensor Technology P.O. Box 1165 SE-581 11 Linköping	FOI-R--0315--SE	Scientific Report
	Research area code 4 C4ISR	
	Month, Year December 2001	**Project no.** E 3026
	Customers code 5. Commissioned Research	
	Sub area code 43 Underwater Sensors	

Authors/s (editor/s)	
Fredrik Kullander	**Project manager** Fredrik Kullander
	Approved by Svante Ödman
	Sponsoring agency Swedish Armed Forces
	Scientifically and technically responsible Fredrik Kullander

Report title
Code Division Multiplexing in Networks of Interferometric Optical Fiber Sensors

Abstract (not more than 200 words)
Code Division Multiplexing (CDM) is found less suitable than other multiplexing methods, e.g.time division multiplexing or frequency division multiplexing, for high resolution interferometric sensor networks since optical field cross-correlation products yield noise that cannot be separated from the sensor signals.
Calculations based on a fundamental approach have been used to simulate the output intensity from networks of interferometric sensors. We have applied the formalism both to a simple optical network, an unbalanced Mach Zehnder interferometer, and to a more complicated nested network of interferometers. The first case was used to show generally how the laser noise convert to intensity noise and to provide insight into how the sensor signal to noise ratio in more complicated networks is related to the laser and network parameters. The more complicated nested network was simulated since it has been intended for use in large scale all optical underwater hydrophone networks. CDM was applied to the network and the output intensity characteristics were investigated. We have performed the numerical calculations with various combination of laser and network parameters. None of the investigated parameter settings were found to give appreciable results. We attribute the negative result to the existence of cross correlation terms in the demultiplexed signals. It was found that the only way to reduce this impact is to use a low coherence laser source. But, even if the use of a low coherence laser source would reduce the cross correlation to a sufficiently low level it would also decrease the tolerable path imbalance of the sensing interferometers. Therefore, it is unlikely that practical systems with acceptable signal to noise and cross-talk conditions can be realized with CDM as the method to distinguish the network sensing elements.

Keywords
multiplexing, code division multiplexing, fiber, fiber optic sensor, network, acoustic sensor, hydrophone array

Further bibliographic information	**Language** English
ISNN 1650-1942	**Pages** 62 p.
	Price acc. to pricelist **Security classification**

Utgivare
Totalförsvarets Forskningsinstitut-FOI
Avdelningen för Sensorteknik
Box 1165
SE-581 11 Linköping

Rapportnummer, ISRN
FOI-R--0315--SE

Klassificering
Vetenskaplig rapport

Forskningsområde
4. Spaning och ledning

Månad, år
December 2001

Projektnummer.
E 3026

Verksamhetsgren
5. Uppdragsfinansierad verksamhet

Delområde
43. Undervattenssensorer

Författare/redaktör
Fredrik Kullander

Projektledare
Fredrik Kullander

Godkänd av
Svante Ödman

Uppdragsgivare/kundbeteckning
Försvarsmakten

Tekniskt och/eller vetenskapligt ansvarig
Fredrik Kullander

Rapportens titel
Koddelningsmultiplexering i interferometriska fiberoptiska sensornätverk

Sammanfattning (högst 200 ord)
Koddelningsmultiplexering (CDM) har funnits vara en mindre lämpad multiplexeringsmetod i högupplösande interferometriska sensornätverk på grund av att optiska korrelationsprodukter ger upphov till brus och störningar som inte kan särskiljas från sensorsignalerna. Andra lämpligare metoder är exempelvis tidsdelningsmultiplexering och frekvensdelningsmultiplexering.
Beräkningar utgående ifrån fundamentala laseregenskaper har gjorts för att simulera ljusintensiteten ut från interferometriska sensornätverk. Simuleringarna genomfördes för ett enklare optisk nätverk, en obalanserad interferometer, samt för ett mer komplicerat nätverk av nästade interferometrar. Resultaten från det enklare fallet visar generellt hur laserbruset samt nätverksparametrar påverkar intensitetsbruset på utgången av ett optiskt nätverk. Det mer komplicerade nästade nätverket studerades eftersom det utgör ett fördelaktigt sätt att konstruera storskaliga helt optiska hydrofonnätverk. CDM applicerades på det nästade nätverket och utintensiteten studerades. Beräkningarna genomfördes för ett flertal kombinationer av laser- och nätverksparametrar men ingen kombination gav ett önskvärt resultat. Det negativa resultatet, med ett lågt signal till brusförhållande, kan kopplas till korskorrelationsprodukter i det optiska nätverket. Det enda sättet att minska denna inverkan fanns vara att använda en laser med kort koherenslängd. Men, samtidigt som en sådan laser minskar inverkan av korskorrelationsprodukter så ställer den högre krav på anpassning av väglängder i nätverket.
Slutsatsen fanns vara att det är osannolikt att praktiska system, med acceptabla signal till brusförhållanden och överhörningsegenskaper, baserade på CDM tekniken kan realiseras.

Nyckelord
multiplexering, koddelningsmultiplexering, fiber, fiberoptisk sensor, nätverk, akustisk sensor, hydrofonnätverk

Övriga bibliografiska uppgifter

Språk Engelska

ISNN 1650-1942

Antal sidor: 62 s.

Distribution enligt missiv

Pris: Enligt prislista

Sekretess

1. Introduction 7

2. Basic principle 7

3. Code generator 9
3.1 Code properties 12

4. Correlation 13
4.1 Crosstalk 16
4.1.1 Zero light intensity condition 16
4.1.2 Offset adjustment 16
4.1.3 Band limited PRBS 17
4.1.4 Slope effects 19
4.1.5 Mixing products 21
4.2 Remarks on this section 24

5. Network of intensity modulating devices 25

6. Simulations of interferometric networks, framework 27
6.1 Solution 30
6.2 Matlab program 32

7. Numerical results for a single unbalanced Mach-Zehnder interferometer 34
7.1 Changing the laser frequency noise spectral density 35
7.2 Changing the interferometer path length difference 37
7.3 Final remarks on this section 38
Resultsheet A 40
Resultsheet B 42
Resultsheet C 44
Resultsheet D 46
Resultsheet E 48
Resultsheet F 50

8. Numerical results for a nested interferometer network 52
8.1 Passive network 52
8.2 PRBS amplitude modulated light applied to the network 53
8.3 Applied signal on one of five sensor coils 54
8.4 Applied signal and PRBS amplitude modulation 55
8.4.1 Demultiplexed signal 56

9. Conclusions 59
9.1 Concluding remarks 61

10. References 61

1. Introduction

Code Division Multiplexing (CDM) is a useful method to address optical fiber sensors in remote networks by means of a single optical carrier [1,2]. Time, wavelength and frequency division multiplexing are other principles having obtained much attention [3]. A distinguishing characteristic of CDM is the efficient use of the optical power but the method may suffer from an increased level of noise, particularly when used in interferometric systems [4]. Effects of polarisation and noise processes have become rather well understood and the technology has reached a certain state of maturity. However, the inherent optical noise properties of a coherent CDM network have not yet been described in detail.

Our past studies of CDM for fiber optic networks of intensity modulating devices [5] revealed that sensor-sensor crosstalk levels in the range of -60 dB are within reach and that a large number of sensor signals can be multiplexed. Our current effort aims to analyse the noise properties of interferometric networks interrogated using this scheme. Typical targeted figures of merits are; phasenoise < 10 μradians/$\sqrt{Hz}$, dynamic range > 80 dB, sensor bandwidth > 5 kHz, sensor to sensor crosstalk < 40 dB, number of sensors in each subarray > 30.

This report include numerical calculations of the optical intensity power spectrum as measured at the output of an optical network and do not cover experimental results from measurements on a CDM network.

The report has a focus on the effects arising in a CDM network but does include noise calculations for a single path-unbalanced Mach Zehnder interferometer since important effects are more easily understood in this case. The effects encountered in a larger network with lots of interconnects are more complex and the origin of all effects not readily understood.

2. Basic principle

At the top of figure 1 one kind of nested interferometer network is shown. This topology is attractive since a minimum number of couplers are required. Light beams passing through successive paths in the ladder array mix finally at the output of the compensating interferometer from which two-beam interference signals corresponding to each sensing coil can be discerned (owing to the increased time delay experienced, moving up the ladder). An alternative to the nested configuration, shown in the bottom of figure 1, is a simpler optical configuration with

parallel MZ-interferometers. This configuration has been considered for initial evaluations with a network of 4 sensors.

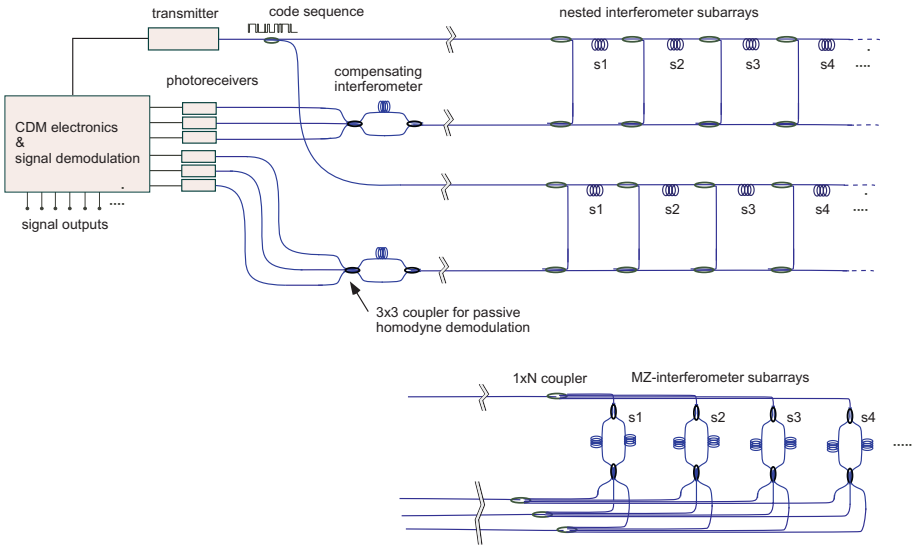

Figure 1 *Nested fibre optic interferometric network. Code division multiplexing, CDM, can be used to address sensors, s1 s2 etc., in each subarray. Alternatively, the subarrays may be configured with individual Mach-Zehnder interferometers.*

A pseudo random binary sequence (PRBS) modulates the output intensity between states of light on and light off, e.g. using a bit period of 100 ns. In parallel the PRBS is electronically delayed to provide synchronous detection at correlator circuits following the photo receivers. The correlators effectively extracts the signals for which synchronization between the optically and the electronically delayed sequence is established. Other signals are suppressed. A 3x3 coupler can be used, as in these schemes, to allow for passive homodyne demodulation of the interferometer signals [6]. A nested network, as shown above, is arranged so that the successive fields in the ladder experience a relative time delay matching the time delay, $\tau_d = nl/c_0$, associated with the path imbalance of the compensating interferometer. Generally, in order to reduce the noise it is important to adjust all fiber path lengths to the best possible precision.

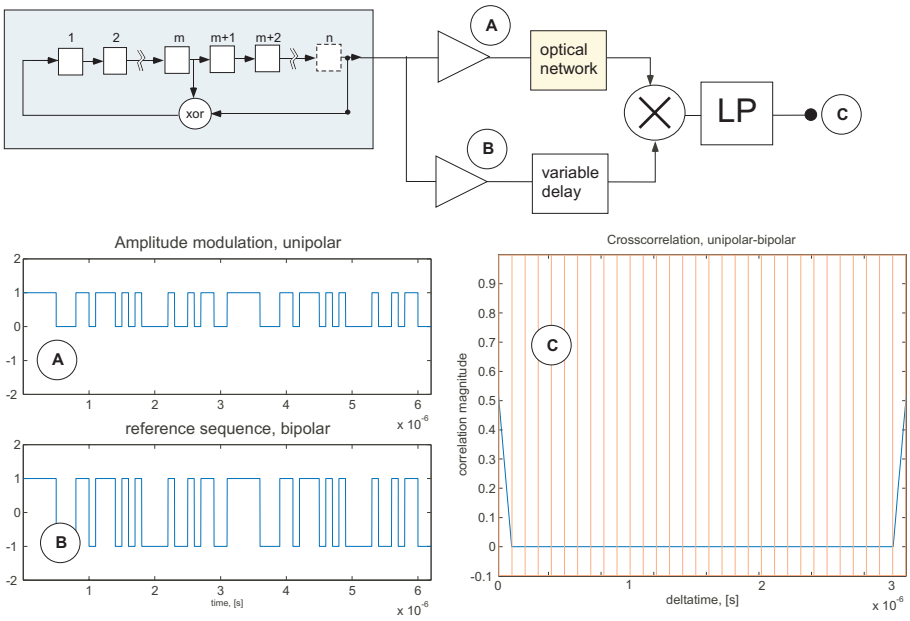

Figure 2 *Basics for CDM in optical fiber sensor networks. PRBS signals may be generated by the use of shift registers with feedback. In this example, m=1 and n=5 yield a sequence of 31 bits. The bit period is 100 ns. A bipolar sequence is used in the electronic branch to obtain the lowest possible crosstalk (zero correlation strength at non synchronized delays). This sequence length allows for 15 completely isolated channels. More channels are accommodated by increasing the sequence length.*

Typical lengths, *l*, that are going to be encountered are in the range 10-100 meters. A precision better than 0.5 cm is hard to achieve.

Our prime interest is to determine the optical noise and subsequently the signal-to-noise ratio and the detection threshold for signals imposed to the system. In the first case we shall assume that the signal to be monitored is a frequency modulation of the laser source while in the second case the signals are length modulations in the network. Since the latter case deals with a multitude of sensor signals it is also necessary to distinguish between them in the network. Code division multiplexing is applied to the network in order to separate the signals. In addition to the noise analysis we shall also calculate the crosstalk between the sensor channels.

3. Code generator

Pseudo Random binary sequences (PRBS) are generated by shift registers implementing what mathematics people call a recurrence system. The output of the register is continually fed back to generate the next output. Linear feedback by means of exclusive or (XOR) gates is com-

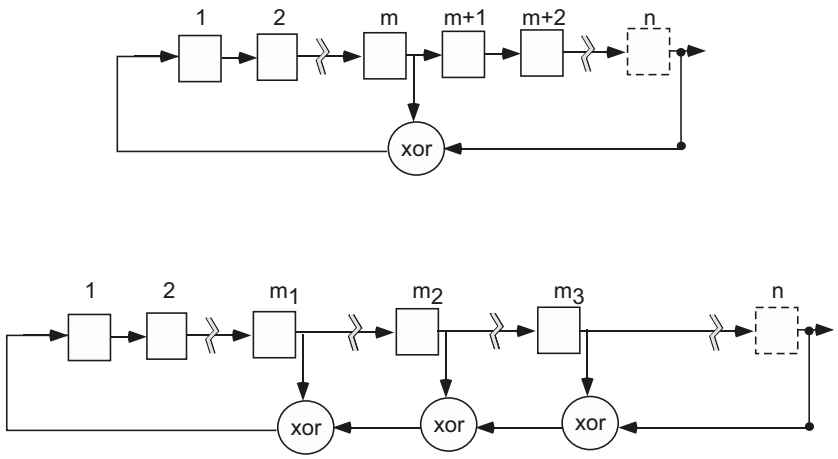

Figure 3 *Linear feedback, n-length shift registers. The choice of feedback taps, m, is crucial for the output. Several feedback taps may have to be used in order to generate m-sequences.*

monly used. A shift register sequence repeats itself after a fixed number of outputs. The largest you can get this number to be is related to the feedback taps and the number of cells. The longest possible is found by length $M=2^n-1$ where n is the number of cells. A so called maximal sequence (m-sequence) is found for certain choice of the feedback taps. A non-maximal setup will produce several (shorter) sequences, depending on the initial state of the shift register. The summed length of all these shorter sequences will be equal to the length of an m-sequence with the same number of shift register cells. A non-maximal set up does not possess ideal correlation properties which is the reason to search for m-sequences. Table 1 summarizes tested configurations resulting in m-sequences based on the topmost shift register shown in figure 3. For

n	2^n-1	m
3	7	1,2
4	15	2
5	31	2,3
6	63	1,5
7	127	1,3,4,6
8	255	-
9	511	4,5
10	1023	3,7
11	2047	2,9
12	4095	-
13	8191	-
14	16383	-
15	32767	1
16	65535	-

Table 1: PRBS choice of feedback taps for the generation of m-sequences.

some of the shift registers, n=8, 12, 13, 14 and 16, m-sequences could not be generated with only two feedback taps. For n=8 it was possible to find m-sequence generators by the use 4 feedback taps arranged as in the lower shift register in figure 3. The shift registers with n=12, 13, 14 and 16 were not tested.

n	2^n-1	m1	m2	m3
8	255	4	3	2
8	255	5	3	1
8	255	5	3	2
8	255	6	3	2
8	255	6	5	1
8	255	6	5	2
8	255	6	5	3
8	255	6	5	4
8	255	7	2	1
8	255	7	3	2
8	255	7	5	3
8	255	7	6	1

Table 2: PRBS choice of feedback taps for the generation of a length 255 bit m-sequence.

3.1 Code properties

Some of the codes generated by the shift register and their power spectrum are shown in figure 4. The PRBS modulation results in a spread spectrum. Spectral peaks distribute equidistantly from the cycle repetition rate up to the clock frequency (10 MHz in this case). Above the clock frequency side lobes following a sinc functional behaviour appears. Minima are found every multiple of the clock frequency. The lower the cycle repetition rate, i.e. the longer the sequence, the more distributed becomes the power within each lobe. When a signal is applied as an amplitude modulation of lower frequency its power will distribute as side bands around the spectral components of the PRBS code. Hence, the PRBS shall be regarded as a spread spectrum carrier. In the case of unipolar modulation the code states of zero remain unmodulated while the one states change value according to the signal modulation. Effectively, the signal modulation can be regarded as an amplitude modulation of the PRBS carrier on top of

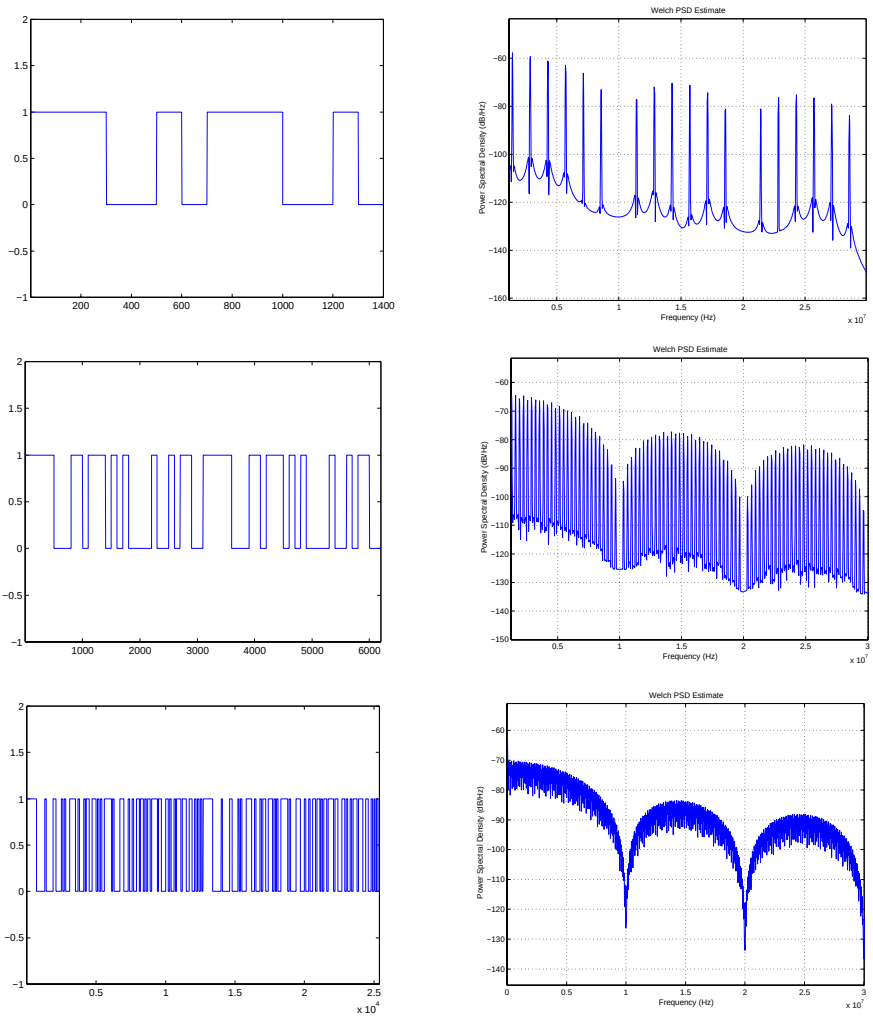

Figure 4 *PRBS codes. The left hand time diagrams display two cycles of the code generated with n=3,5,7 respectively. The right hand diagrams shows spectra of the ideal unipolar PRBS.*

direct modulation of the intensity. Therefore the signal will appear both as sidebands around the carrier and in the base band as seen in figure 5. The spectrum of an ideal unipolar PRBS,

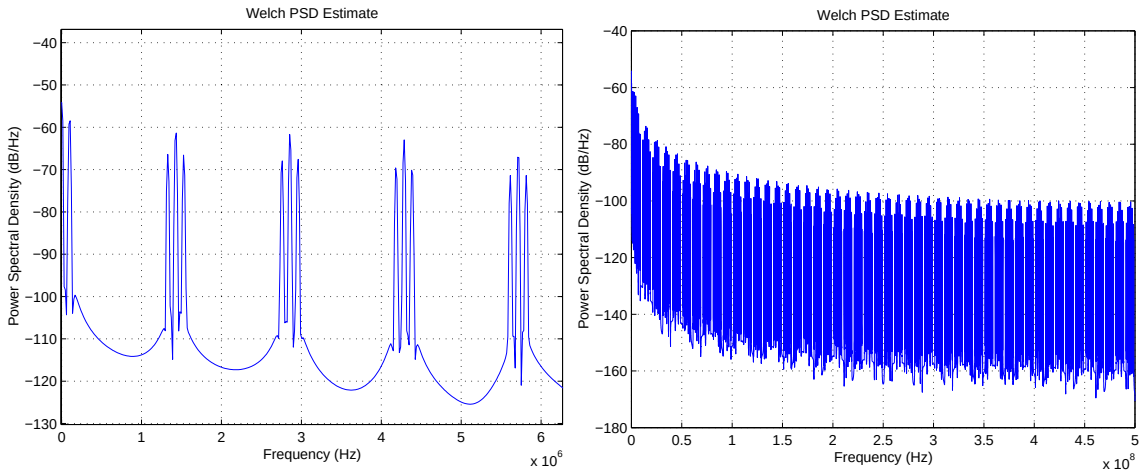

Figure 5 *Spectrum of an ideal unipolar PRBS of 8 bit length modulated by a sinusoidal signal at 100 kHz. The signal appears both in the baseband and as sidebands around the PRBS carriers.*

generated with n=3 (bitlength=8) take on the character of a sinc function seen in a broad bandwidth. A closer look at lower frequencies reveals that sidebands appear around the PRBS tones and that the signal is visible in the baseband. Upon demodulation using a bipolar reference code the baseband component will be averaged out and does not contribute to the demultiplexed signal. Hence, the power contained around the spectral components of the PRBS carrier is the signal power which is used.

4. Correlation

In our set-up the m-sequence modulates the laser on/off at 10 MHz and is also delayed electronically to provide synchronous detection at the correlator circuit. The electronically delayed sequence, $h(t-\tau_j)$, is bipolar, i.e. its binary values represent +1 and –1 states. The detected optical power can be written as

$$P(t) = \sum_{i=1}^{N} P_i(t)h'(t-\tau'_i) \qquad (3)$$

where N is the total number of sensors, $P_i(t)$ is the part of the detected power transmitted through the sensor coil denoted "i" and $h'(t-\tau'_i)$ is a unipolar PRBS, which in contrast to the bipolar sequence has binary values ideally represented by 1 and 0. Finally, τ'_i is the time delay experienced by the sequences travelling through each sensor.

To demultiplex the sensor signals, modulated onto $P_i(t)$, the detected optical signal is correlated with the electronically delayed sequences. In this way, the sensor signals can be simultaneously recovered by means of one channel with a correlator circuit (here a multiplier and a low-pass filter) for each sensor. If $P_i(t)$ are assumed to be slowly varying signals compared to the code word repetition rate, 1/MT, the correlator output voltage can be approximated by

$$V_j(t) \approx \sum_{i=1}^{N} GP_i(t)R_{h'h}(\tau) \tag{4}$$

where

$$R_{h'h}(\tau) = R_{h'h}(\tau_i' - \tau_j) = \frac{1}{MT}\int_0^{MT} h'(t-\tau'_i)h(t-\tau_j)dt \tag{5}$$

Here G is the overall conversion gain of the receiver. M is the length of the m-sequence in units of bits and T is the bit period.

The cross correlation of the unipolar and the bipolar m-sequence is ideally

$$R_{h'h}(\tau) = \begin{cases} \frac{1}{2}\left(1+\frac{1}{M}\right)\left(1-\frac{|\tau - nMT|}{T}\right), |\tau - nMT| \le T \\ 0, \text{otherwise} \end{cases} \tag{6}$$

with n= 0, ±1, ±2,... Therefore the correlator effectively extracts the signal $P_j(t)$ from the sensor for which synchronization is established, i.e. when $\tau = nMT$, and the correlator output voltage becomes $V_j(t) \approx 0{,}5GP_j(t)$. So, the different sensor signals appear at different channels. Signals carried by non-synchronized sequences are averaged to zero in the correlators, a

unique feature of the unipolar-bipolar correlation function. A unipolar-unipolar correlation will also suppress non-synchronized signals but has not got the property of total rejection.

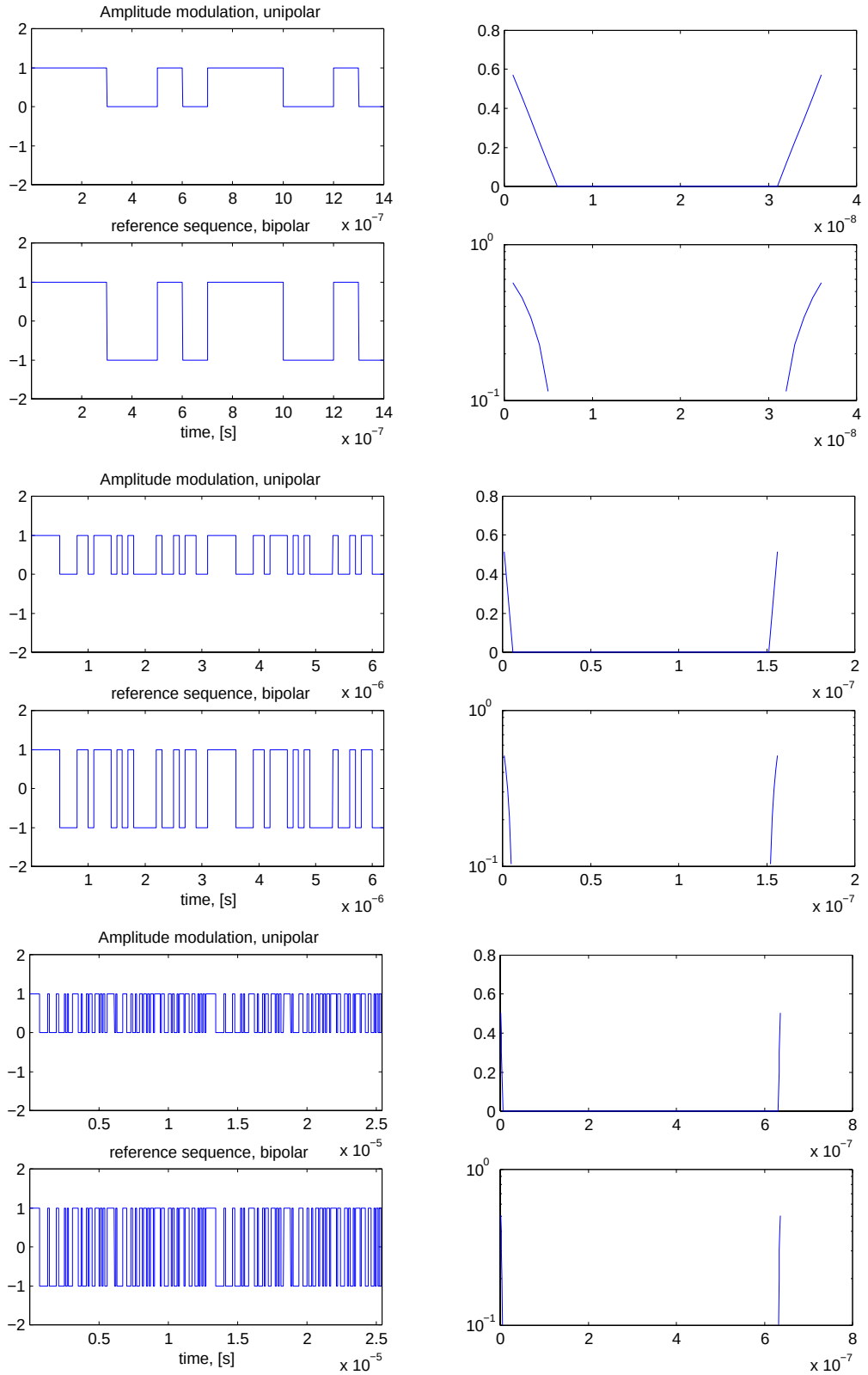

Figure 6 *PRBS code correlation properties. Cross correlation functions between unipolar and bipolar sequences with n=3,5,7 respectively are shown to the right. The absence of values in the logarithmic diagrams indicate that the value is actually zero.*

4.1 Crosstalk

Crosstalk between sensors arises if the correlation function for some reason departs from zero for non-synchronized delays. In practice, non-ideal properties of the m-sequences give rise to crosstalk. The ideal cross correlation diagrams are shown in figure 6 for three different sequences. The correlation magnitude has its maximum of about 0.5 at synchronization and then drops off towards zero according to equation (6). The shorter the sequence the more time-lag is occupied by the channel. In order to completely isolate adjacent channels they must be separated by 2T. Under this condition we realize easily that more channels can be accommodated by the use of longer sequences. But, at the same time the frequency band allowed for the signals becomes lower since the PRBS spectrum occupies lower frequencies. For example, using a clock frequency of 10 MHz, a 31 bit sequence allows for 15 channels with a 160 kHz bandwidth and a 255 bit sequence allows for 127 channels in a 20 kHz bandwidth.

4.1.1 Zero light intensity condition

If low crosstalk is desired in fiber optic sensor system unipolar-bipolar code mixing should be used. Then, perhaps the most essential condition to assure is that the light intensity is close to zero for logical zero states in the unipolar sequence. The remaining light in the logical zero states can be regarded as a continuous intensity propagating the sensor signals to the detector independent of the PRBS coding, which will result in crosstalk. Moreover the code polarity must be turned such that an even number of logical one states are obtained. The number of bits in on cycle of the PRBS is always odd and it is possible to modulate the light intensity with the wrong code polarity in this respect. Proper conditions as above allows for zero correlation at non-synchronized delays.

4.1.2 Offset adjustment

Another significant factor is the detailed properties of the pulses. Although both the shape of the intensity unipolar modulation and the reference bipolar modulation must be adjusted with care one may focus on the bipolar sequence under the condition that the light is truly zero during the full logical zero states. It is very important to carefully adjust the bit time values, the rise- and fall-times, and the voltage offset levels. The offset adjustment can bee used for fine tuning (balancing) of the bipolar sequences to reach low crosstalk conditions. Let us for a while assume that the unipolar code is ideal and consider non-ideal properties of the reference bipolar code.

If the bipolar sequence, ideally switching between values of -1 and 1 (may be regarded as voltage levels), is not perfectly symmetric around 0 the correlation magnitude at non-synchronized delays will increase significantly. Offset levels ranging 0 to 0.2 in steps 0.02 have been added to the bipolar code. The correlation magnitude, as shown in figure 7, is critically dependent on the offset. It reaches a level of 10^{-2}, corresponding to a sensor to sensor crosstalk level of -40 dB, already for an offset of 0.02. Hence, it is very important to balance the bipolar sequence. A

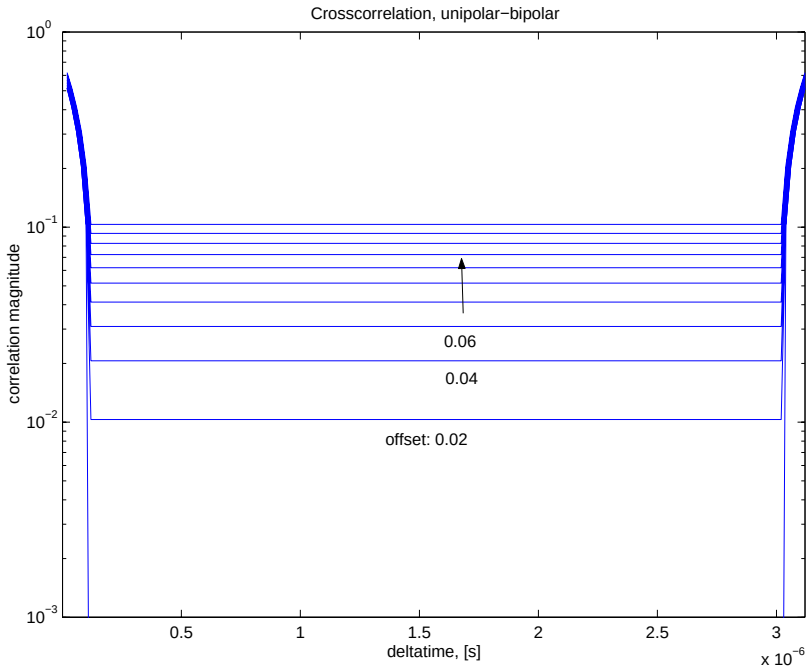

Figure 7 *Cross correlation of a unipolar sequence with a bipolar sequence being offset in steps of 0.02.*

precision better than 1/100 is required. This can indeed be met in practice but probably not without means for offset tuning in the electronic circuitry.

4.1.3 Band limited PRBS

Another property of the code sequence often faced in a practical system is that it is bandlimited. If we assume that the electronic circuit behaves as a linear network (not always true in practice) incorporating frequency dependence the net effect of the network can be modelled as a filter with a linear transfer function. We have applied a low pass filter to the PRBS code to simulate a band limited electronic network. As can be seen in figure 8 a filter with an edge frequency well above the clock frequency does not have any serious effect on the cross correlation. Neither if the edge frequency is decreased to 11 MHz.

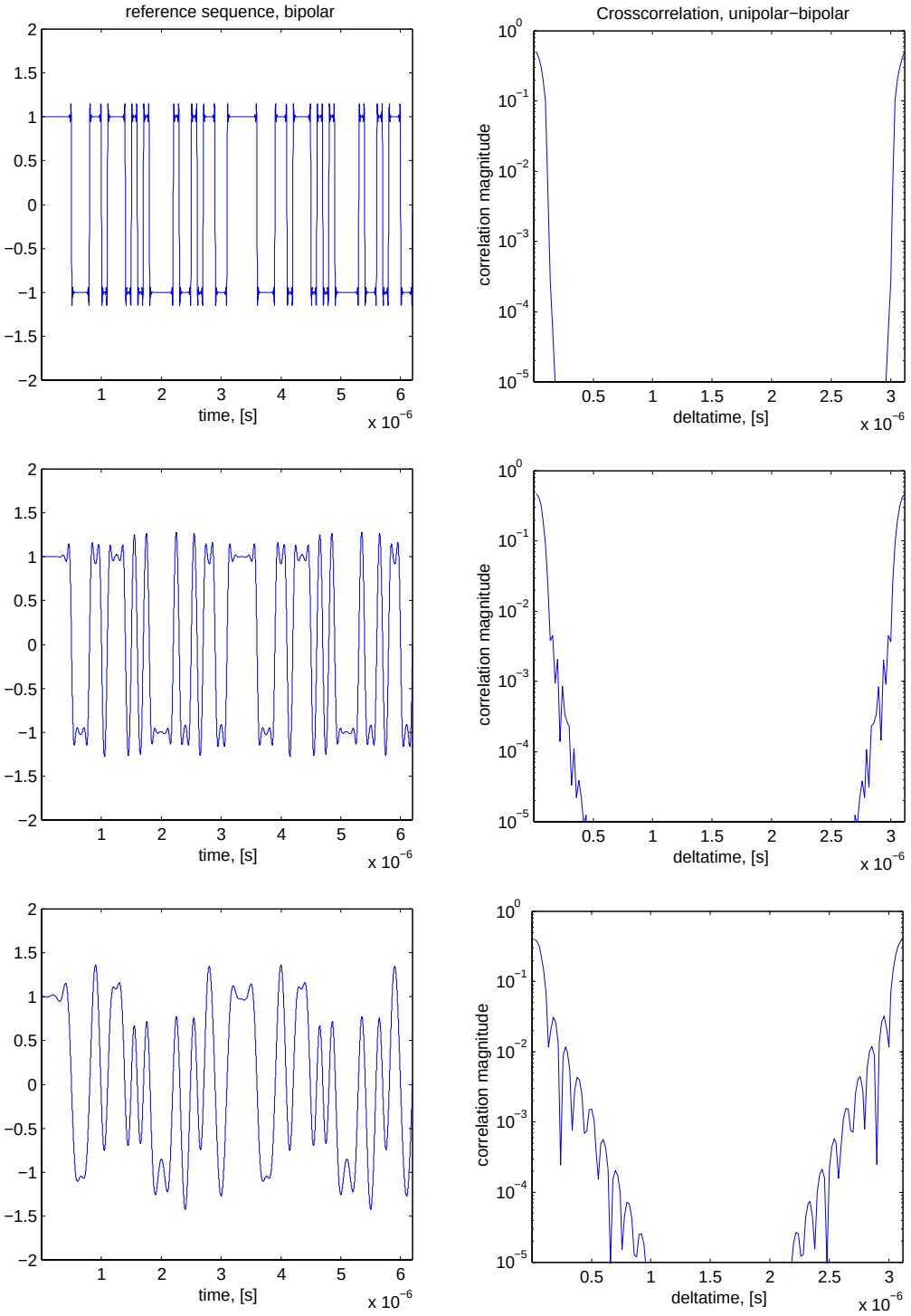

Figure 8 *Filtering applied to the bipolar PRBS. From the top to the bottom a Butterworth IIR low-pass filter of 5th order with edge frequency set to 50, 11 and 5 MHz respectively. Cross correlation with an ideal unipolar sequence is shown to the right.*

However, the correlation amplitude increases around the synchronization condition and we see that the channel spacing may have to be increased to keep a certain level of crosstalk. If the edge frequency is decreased further beyond the clock frequency the cross correlation at non synchronized delays becomes further enhanced and the demultiplexing may not work satisfactorily. Note that we are only dealing with the bipolar sequence. A corresponding band limitation of the unipolar sequence would lead to enhanced crosstalk since a part of the logical zeros would carry optical information. But, for the case of the optical carrier this problem can be overcome by altering the duty cycle of the code such that the logical one states are made slightly shorter than the zeros. In that way the slopes associated with the logical state switches are moved into the domain of logical ones while the light intensity is kept zero during the duration of the logical zeros.

The low crosstalk levels obtained with the filter set to 11 and 50 MHz are not obvious. It can be explained by symmetry. Zero cross correlation can be obtained since the bipolar states for non synchronized delays distributes with an equal amount of positive and negative states over the unipolar one states. Hence, as long as the positive and negative states are represented by pulses for which the absolute value of the instantaneous amplitude follow identical curves, slope and distortion effects cancel out. The careful reader may notice that the pulse shape associated with a single bit will also depend on the states of the neighbouring bits. A slope on either side of the bit is present only if the state is changed in either direction. Not obviously, it turns out that also the different type of pulses are equally distributed about the unipolar one states and the edge effects always cancel out. Even for delay-times which are not multiples of the bit period. In conclusion, we have found that the crosstalk does not increase dramatically when a linear filter is applied to an ideal bipolar PRBS.

4.1.4 Slope effects

We have seen that a linear filter distorts the two bipolar states in a symmetric fashion. The same effect is illustrated in figure 9 where an ideal bipolar PRBS is being modified with edge slopes. The rise and fall times are changed equally much from 5 to 50 ns. In this case the resulting cross correlation is approximately independent of the rise and fall times. In practice, non-linear effects may lead to slopes which are dependent on their sign. That is, if it is a posi-

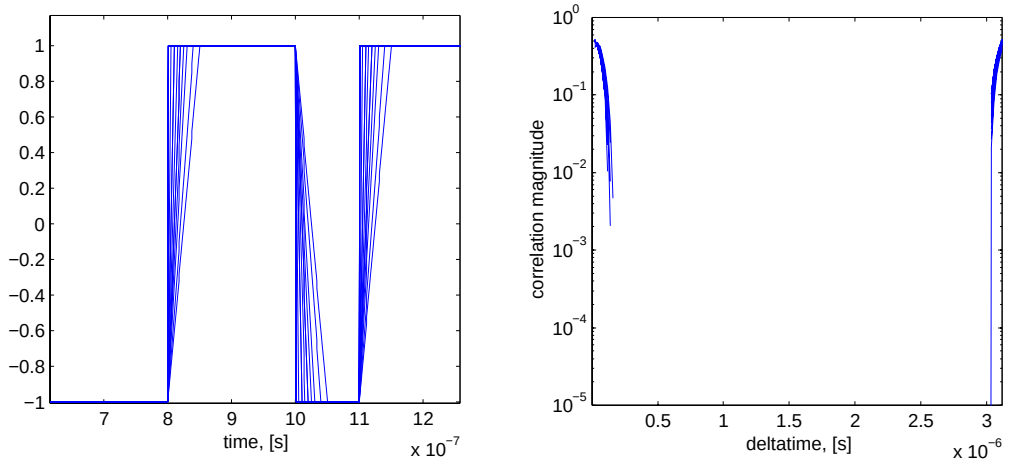

Figure 9 *Altered slope at state changes. Left hand diagram shows 10 bipolar sequences with their rise and fall times are being modified equally from 5 to 50 ns. The right diagram describes the correlation between the modified bipolar sequences and an ideal unipolar sequence.*

tive or negative edge. For such cases the above argumentation does not hold and it is going to be more difficult to obtain low cross correlation for non-synchronization. As seen in figure 10 where only the rise time is modified the cross correlation magnitude for non-synchronized delays increases dramatically. The slower the rise time the higher the cross correlation magnitude. The peak appearing in the middle of the correlation diagram has unknown origin. It may result from approximations or some other error in the calculations. A physical explanation has not been found. The main thing to learn from this simulation, however, is that the level of crosstalk is critically dependent on the positive edge slope. Unless the negative slopes follow

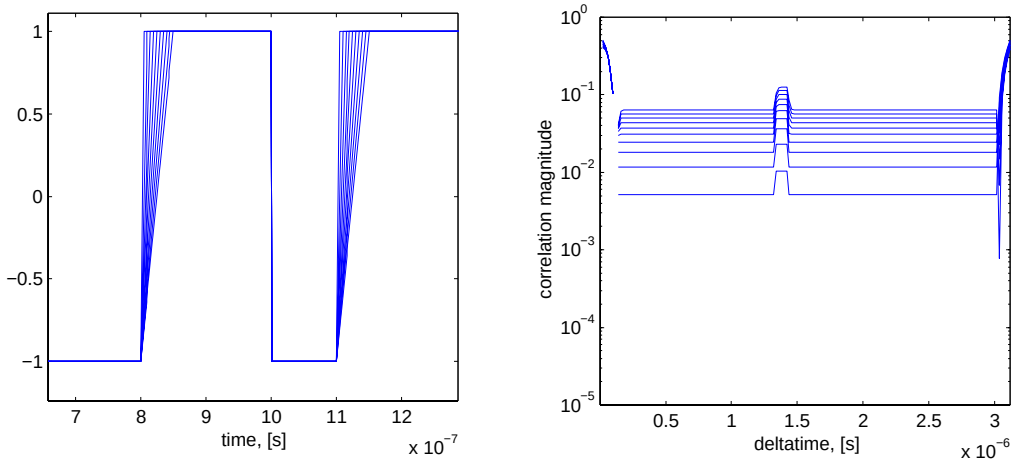

Figure 10 *Changing the slope. Left hand diagram shows 10 bipolar sequences with their rise and fall times are being modified equally from 5 to 50 ns. The right diagram describes the correlation between the modified bipolar sequences and an ideal unipolar sequence.*

the same pattern a finite rise time may lead to unacceptable crosstalk. A way to reduce the cross correlation for this last case is to compensate the generated asymmetry by applying a low level of offset. We show in figure 11 that the cross correlation can be reduced by shifting the bipolar sequence. The bipolar sequence modified to incorporate 50 ns rise times was offset in steps of 0.01 (dimensionless units) and it was found that a minimum cross correlation magnitude at a level of about 10^{-3} was obtained when the offset was 0.06. It was not possible to completely eliminate the cross correlation. Nevertheless we see that it is possible to compensate non-ideal pulse shapes to a certain degree by applying an offset. We believe that the optimum is reached when the offset is adjusted so that the integrated power of the signal in each logical state equalizes.

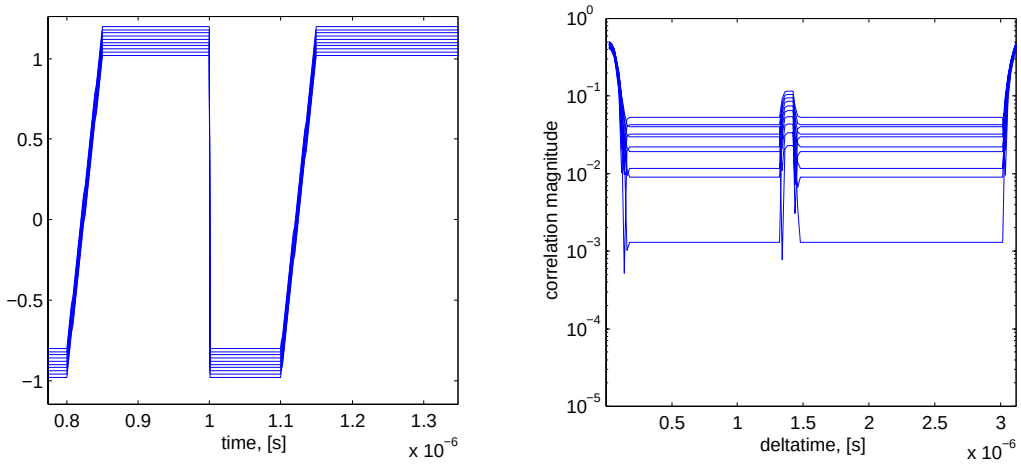

Figure 11 *Left hand diagram shows the bipolar sequence a one sided 50 ns slope with offset being modified from 0 to 0.1 in steps of 0.01. The right diagram describes the correlation between the modified bipolar sequences and an ideal unipolar sequence. The lowest level of cross correlation is reached at an offset of 0.06 for this particular case.*

4.1.5 Mixing products

Mixing products in this context refer to the optical interference products arising in a coherent network. We address this subject since we believe that the unwanted mixing products and their net effect on the demultiplexed output signals may be the most difficult problem to overcome. When an interferometric fiber optic sensor system is excited by coherent light the mixing products will arise everywhere where light beams are brought together. In fact, the two beam interferometers constituting the sensors will deliver the signal information in form of a mixing product. The main concern here is that a multitude of beams differently delayed will mix and generate mixing products of non synchronized modulation. The aim for the sensing interfer-

ometers in this kind of systems is almost always to keep the path imbalance as short as possible in order to keep down the phase noise. Therefore the mixing product associated with the sensing interferometers are generated at synchronization. The non-synchronized mixing products are carrying codes with two different delays and we may expect synchronization at both these delays. A simple test where two identical unipolar, 31 bit length, sequences have been multiplied at different relative delays followed by a correlation with a bipolar reference sequence has been performed. A series of correlation diagrams are shown in figure 12. The relative delay between the signals was varied in steps of 40 ns. An expected behaviour is that an additional correlation peak corresponding to the delayed sequence follows the applied time delay. The peak can be seen moving from 0 to 360 ns in steps of 40 ns. Less obvious is that secondary peaks develop at time delays which can not easily be associated with the applied time delay. As the differential delay is increased these secondary peaks follow a pattern of first appearing at two different time lags. While the correlation magnitude increase in one peak it decreases in the other. When the correlation magnitude in one of the peaks reaches a maximum at 0.25 the other peak disappears. When the time delay is further increased the remaining secondary peak starts to decrease while a peak at another time delay develops. Clearly, the mixing products will yield unwanted cross correlation.

How does this affect the noise and crosstalk properties of the demultiplexed signals? If we consider the channel corresponding to synchronization in the correlation diagrams;

-Firstly, it will be correlated with the mixing products in which one of the factors is synchronized with the reference code although the correlation magnitude is only half of that for the wanted signal. Thus if N beams with different delays are mixed in the network N-1 unwanted mixing products appears at each output.

-Secondly, the additional peaks appearing in the correlation diagrams may interfere with other channels. In the same way, additional correlation from mixing products in which neither of the two factors is synchronized with the reference code may develop. The shorter the PRBS the more likely it is that this kind of additional interference appears.

These mixing products will indeed contain sensor signal information but may also carry noise due to the comparably large interferometric path imbalance they represent. Both the potential

sensor to sensor crosstalk and the noise makes it necessary to reduce their impact. The only way to do that is to reduce the coherence length of the laser source in order to reduce the amplitude of the unwanted mixing products. We will discuss this in the following section.

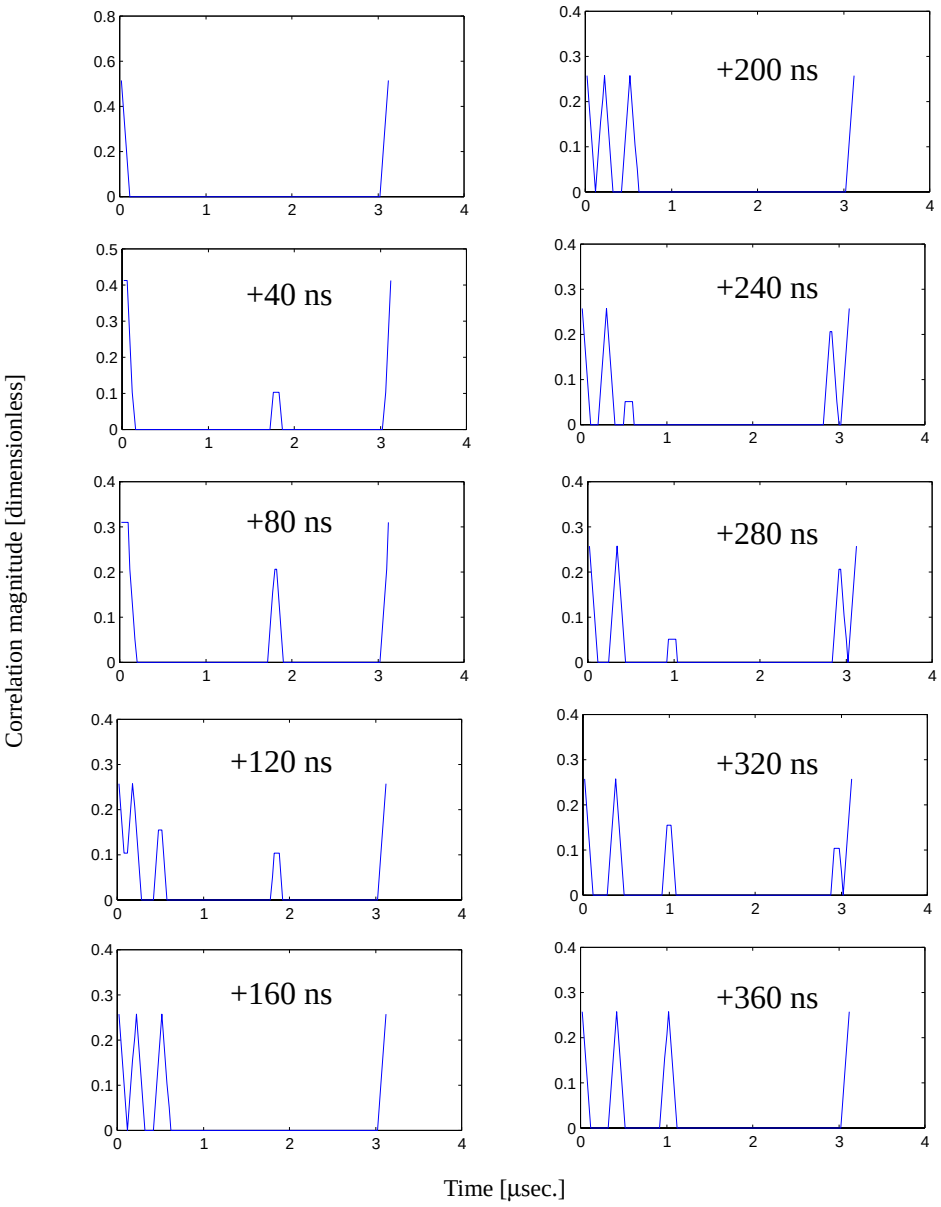

Figure 12 *Two mixed unipolar PRBS codes correlated with a bipolar reference code. The correlation diagrams shows the result upon variation of the time delay between the two unipolar mixed sequences. The time delay is zero in the upper left diagram and increased in steps of 40 ns.*

4.2 Remarks on this section

The level of cross correlation when a unipolar and a bipolar PRBS are mixed has been shown to be ideally zero for non-synchronized delays. This inherent property can be used to achieve very low crosstalk between sensors in a fiber optic network. In practice however there are several effects which can increase the unwanted cross correlation as has been shown in this section.

5. Network of intensity modulating devices

CDM has been shown previously [5] to be a useful method in ladder networks of intensity modulating devices. For the purpose of illustration and introduction to the forthcoming chapter we show here simulated results for an intensity modulated network. The topology of a ladder network is shown in figure 13. A transmitter may be directly modulated or by means of an

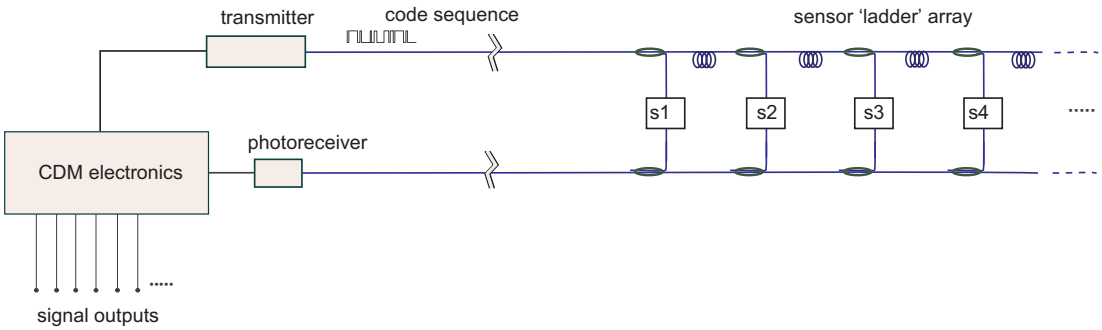

Figure 13 *Ladder network of intensity modulating sensors with CDM multiplexing.*

external modulator with a continuous PRBS code switching the light between states on and off. The CDM electronics include delay and correlator components. We have simulated the output of this network with three sensors. Sinusoidal signals at frequencies of 40, 55 and 90 kHz were applied to the three sensors respectively. The light source was assumed to be completely incoherent and a RIN level of -120 dB was used. A PRBS code with n=5, yielding 31 bit length m-sequence was used. The power spectra depicted in figure 14 are scaled with reference to the network input power. Characteristic features as discussed in chapter 3 are that the detector signal contains the sensor modulations both in the baseband and as sidebands around the PRBS harmonics. The baseband signals do not contribute to the demultiplexed signal and could have been rejected by a highpass filter. The demultiplexed signals are shown after multiplication with bipolar sequences synchronized with the respective sensors. The final signal is obtained by passing the signal through a lowpass filter in order to reject the PRBS harmonics. We see that each sensor modulation appears at their respective channel and that crosstalk is completely eliminated. Of course, the conditions are ideal in this example. In reality, great care has to be taken to reach crosstalk levels below -60 dB. But as we have shown earlier this is indeed possible.

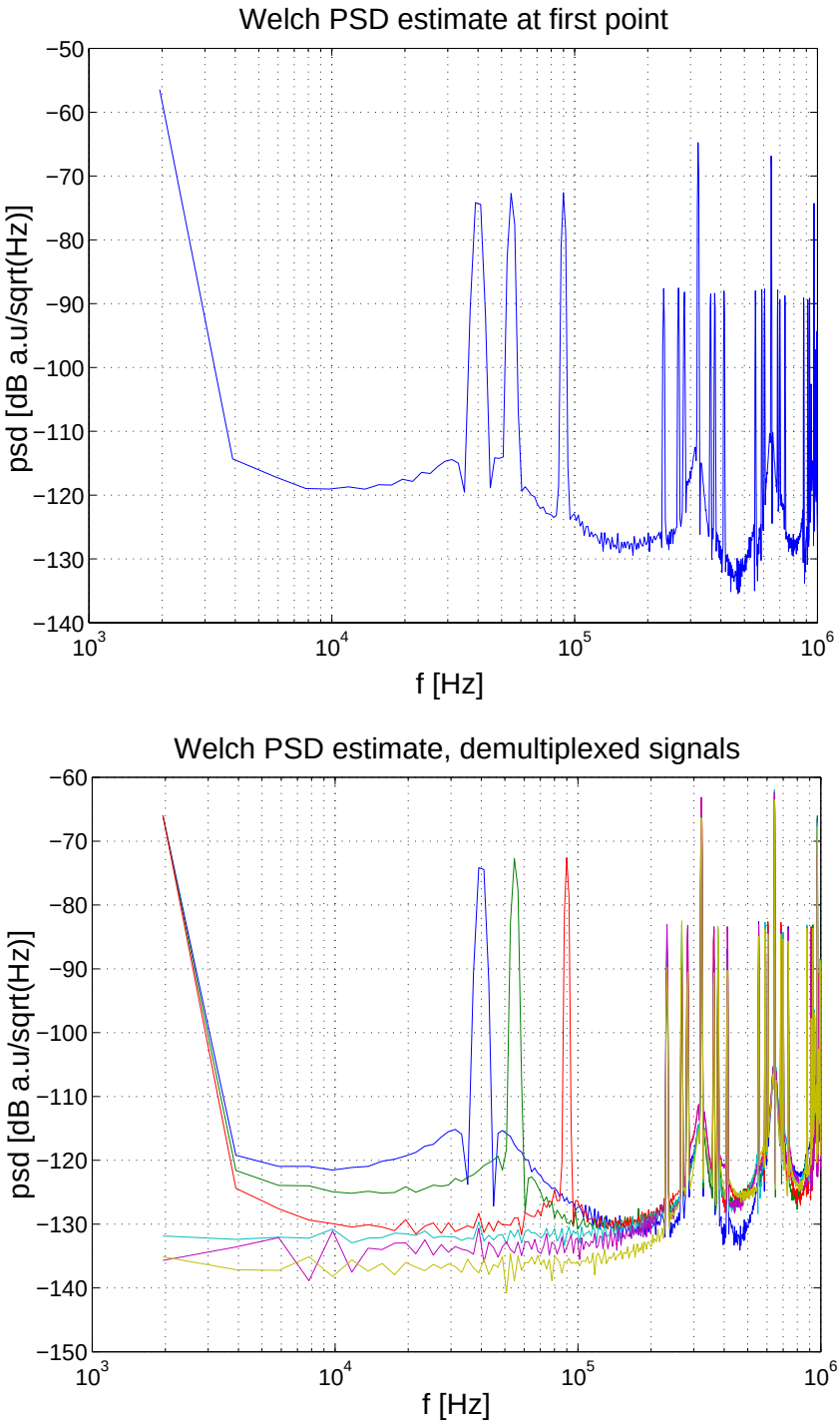

Figure 14 *Power spectrum of the detected optical signal in the top diagram and of the demultiplexed channels in the bottom diagram.*

6. Simulations of interferometric networks, framework

Interferometric networks are much more complicated to describe in detail since the optical fields add up and interfere in network joints. The way in which interference takes place is critically dependent of the statistics of the laser source and it has been necessary to describe how the signals add and propagate in the network from a rather fundamental point of view. A great deal of this chapter is set aside to describe the noise properties of the network. Since CDM applied to interferometric networks will have to rely on rejection of cross mixing products by the use of lasers with limited coherence length it is important to clarify what this means for the overall noise appearing in the network.

A Matlab program has been used to calculate numerically the optical output power from two kinds of interferometer networks excited by narrow band (quasi monochromatic) continuous wave (cw) laser light sources. A basic statistical approach has been used to simulate the effects of stationary noise sources. We adopt some general ideas, found in textbooks [7-9], about the inherent noise of single frequency lasers. The intensity noise and the phase noise of the laser are regarded as independent random Gaussian processes, both being stationary and ergodic, thus time independent. The time dependent parameters being introduced later are assumed to be independent of this noise. It is common practice to assume that the fundamental limit of the detection threshold of interferometric systems is set by the noise generated from the frequency fluctuations of the laser, provided the detector noise level is exceeded. The laser source intensity noise will generally give rise to a comparably lower level of output noise and can be suppressed by means of common mode rejection where two or more outputs from an interferometer are coprocessed. Common mode variations can be separated from phase angle modulating signals when each detector monitors the interference signal at different relative phases. Hence, our prime interest is to investigate how laser frequency noise contribute to the output power spectrum of interferometric networks.

We treat one principle polarization mode in fiber optic networks and we neglect the effects of dispersion and birefringence. Moreover we assume that the noise processes involved are Gaussian, motivated by physical arguments, and that the linewidth of the propagating field is narrow compared to its central frequency. The analytical function of the optical field may then be cast in the form

$$u(t) = a(t)\exp(i\phi(t))\exp(i2\pi\nu_0(t-\theta)) \tag{7}$$

where $a(t)$ is the amplitude (taken to be real) of the field, $\phi(t)$ is the phase, ν_0 the central frequency of the optical field, t the local time parameter and θ a random time parameter to account for the physical uncertainty of the time in the detection process. By introducing the random time parameter θ uniformly distributed in the interval $[0, 1/\nu_0]$ we shift the original cyclostationary process to a stationary process, see [7]. Note that we regard $a(t)$ and $\phi(t)$ as statistically independent functions. The local time parameter is referenced to a frame moving along the fiber, in the positive z-direction, with the group velocity of the propagating field. Thus, to describe the field as a function of the time in the laboratory or the z-coordinate the substitution $t = t_l - nz/c_0$ shall be used. Here, t_l is the laboratory time, n the effective refractive index of the propagating mode and c_0 the speed of light.

A useful model of an amplitude-stabilized continuous wave laser field is the random-phase model [7]. In this model it is assumed that the instantaneous optical frequency is time-dependent and can be expressed as a time integral of the instantaneous frequency deviation.

$$\phi(t) = 2\pi\int_0^t \Delta\nu(t')dt' + \phi_0 \tag{8}$$

We shall adopt this model and assume it to be valid in the presence of intensity (amplitude) noise. The amplitude variations are modelled as

$$a(t) = (a_0 + \Delta a(t))m(t) \tag{9}$$

where a_0 is the mean amplitude, $\Delta a(t)$ the amplitude noise and $m(t)$ a modulation function which is introduced to describe the incident field after having passed through an external amplitude modulator driven by the CDM code (not depicted in the first following figures). For an unmodulated cw laser we use simply $m(t) = 1$ .The normalized detected power is

$$P(t) = \langle |u(t)|^2 \rangle \tag{10}$$

where the average is taken over the integration time of the detector. The major task in this report is to express the spectral properties of the detected power as a function of the various parameters affecting it. Throughout this document we have used Welch's method of averaged periodograms to visualize the power spectrum $S(f) = |\tilde{P}(f)|^2$ of the received optical signal *P(t)*. $\tilde{P}(f)$ is the Fourier transform of *P(t)*, here defined as

$$\tilde{P}(f) = \int_{-\infty}^{\infty} P(t)\exp(-i2\pi ft)dt \tag{11}$$

In figure 15 is shown schematically the two analysed networks. The first represents a simple unbalanced Mach-Zehnder (MZ) interferometer coupled to a light source whereas the second larger network shows schematically a MZ interferometer following a ladder arrangement with N number of interconnects moving up along the ladder.

The first network is tested for the purpose of a general illustration of the effects arising due to interference. But, since it is commonly applied to measure laser frequency noise characteristics and since it can be used to detect frequency modulating signals of fiber laser or Bragg grating sensors [10] it serves its own purpose. Moreover, by applying modulating devices in the network we can easily obtain results describing the general characteristics of coherent laser radar systems, excluding effects appearing in the air.

The second network is to be used for interferometric fiber sensors where the sensor signals are made to modulate the optical path length of the interconnects. Interferometric mixing occurs when the paths are reconnected. The final, so called, compensating interferometer is used to

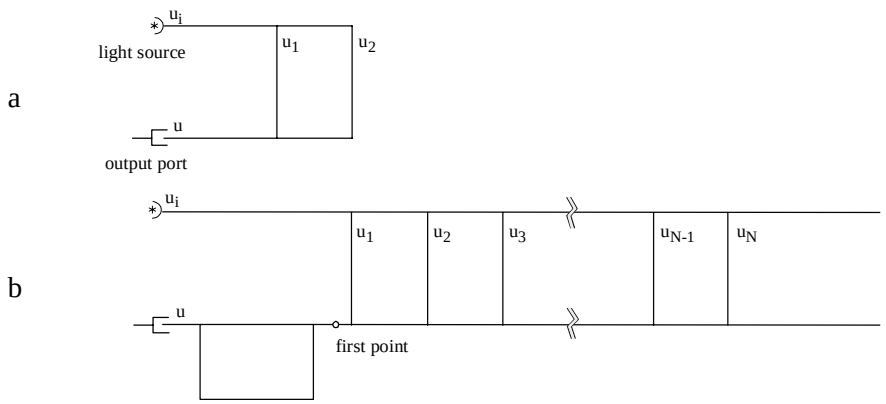

Figure 15 *Schematic drawings of analyzed networks a. unbalanced Mach Zehnder interferometer. b. Nested interferometer network in ladder arrangement and with compensating interferometer.*

compensate for the path imbalance between successive interconnects. An operational system configured in this way is arranged so that the successive fields in the ladder experience a relative time delay which is equal to the time delay, $\tau_d = nl/c_0$, associated with the compensating interferometer.

6.1 Solution

To simplify notation it suffices to use the local time parameter as described above. The optical field is defined both by a subscript denoting which branch it belongs to and a time coordinate defining the local time for each of the fields at particular points in the network. In our cases, the interesting features are found after joints in the fiber network where the field components are added. In the local time frame a forward translation along the room coordinate transforms into a time delay. Hence, in the local time frame the fields are delayed. See figure 16 which

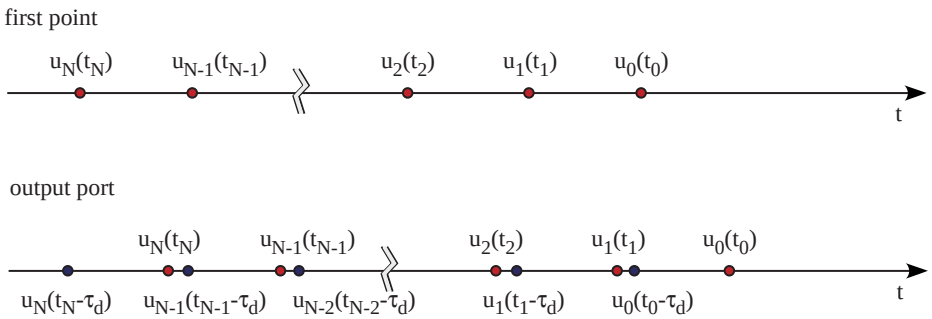

Figure 16 *The optical field translated in the forward direction along a room coordinate is equivalent to the field being delayed in time.*

depicts the fields of the nested network at the first point and at the output port. It is not necessary to include common time delays in the final expression for the purpose of finding the power since such delays do not affect the power spectrum. However, it should be remembered that the total delay must be known when electronical mixing is to be used.

The analytical function of the optical field at the photo detector in the nested network can be written as

$$u(t) = \sum_{k=0}^{N} [u_k(t_k) + u_k(t_k - \tau_d)] \qquad (12)$$

where k ranging *0 to N* denote the ladder interconnects starting from zero at the bottom of the ladder, u_k is the field term propagating through the interconnect k incorporating all network losses, $t_k = t - \tau_k$ and τ_d is the differential time delay associated with the compensating interferometer.

This is generally how far we need to describe the network to be able to calculate numerically the detected optical power provided the statistics of the laser source are incorporated in the field description. Nevertheless it is worthwhile to work through a simplified (ideal) network in which the couplers are chosen so that an equal amount of power propagate through the interconnects and where all field amplitudes are unaffected by the environment and experience equal propagating conditions.

The fields are simply delayed differently while propagating in the network. The sensor signals modulate the delay of each field. In this case $u_k = u_0$ for all k's. Moreover, the time parameter t_k of the field components are set to multiples of τ_d such as $t_k = t - k\tau_d$ (by means of adjusting the fiber lengths). Without signal modulation the output field can be written as

$$u(t) = u_0(t) + 2\sum_{k=1}^{N} u_0(t - k\tau_d) + u_0(t - \langle N+1\rangle\tau_d) \tag{13}$$

and the output power, here defined as $P(t) = \langle |u(t)|^2 \rangle$, becomes

$$P(t) = P_0(t) + P_0(t - \langle N+1\rangle\tau_d) + 4\sum_{k=1}^{N} P_0(t - k\tau_d) + 8\sum_{j=1}^{N-1}\sum_{k=j+1}^{N} R_0(t, \tau_{jk}) + \tag{14}$$

$$\sum_{j=1}^{N} 4[R_0(t, \tau_{j0}) + R_0(t, \tau_{j,N+1})] + 2R_0(t, \tau_{0,N+1})$$

where the cross-correlation terms are given by

$$R_0(t, \tau_{jk}) = \langle u_0^{(r)}(t - j\tau_d) u_0^{(r)}(t - k\tau_d)\rangle \tag{15}$$

The superscripted (r) denotes the real part of the function. The two first terms in equation (14) are simply due to beams propagating through the shortest and the longest path in the network and will not carry interferometric information. The first sum of terms are those which are to be discerned and will be carrying the relevant sensor information. These terms are mixtures of two optical fields having traversed successively delayed paths and can be distinguished in the process of demultiplexing. The remaining (cross-correlation) terms are all other mixing products in the network. They are of serious concern in an interferometric system and require particular attention since they will procure noise originating in the laser and may lead to crosstalk between the sensors.

Unlike in time division multiplexing these terms will not be fully rejected when using CDM. As was discussed in a previous section, when two non-synchronized unipolar PRBS modulated fields are mixed the product becomes correlated with both fields. Moreover, correlation peaks at one or two other delays develop. The correlation magnitude decreases but is still going to be considerable. Hence, to reduce the cross correlation magnitude it is necessary to use a laser with short coherence time, τ_c. If the coherence time is shorter than τ_d the developed noise power becomes approximately proportional to τ_c. Unfortunately, for lasers with ordinary frequency noise characteristics this will inevitably result in an increased level of noise in the sensor channels which will generally increase as $1/\tau_c^2$ within the desired frequency band. It is possible to find an optimum laser for each network but highly coherent lasers are not suitable due to the cross-correlation.

The main task of the following numerical calculations is to provide an understanding of the effects arising from the cross correlation and to find possible way to suppress noise originating in this effect. We shall investigate the available signal-to-noise as well as the crosstalk for a system multiplexed using CDM. First, though, we will make the calculations for the much simpler single unbalanced interferometer (network *a*) in figure 15.

6.2 Matlab program

A program named “coherentnetwork” written in Matlab has been used to simulate the output powers of the above type of networks. Basically, a long discrete input vector $u_i(t)$ describing the source optical field is generated. New delayed vectors, $u_k(t)$ are generated from the input vector and are then summed according to equation (12). The output power is calculated for

user selected input parameters, shown in figure 17. Parameters defining the relative intensity

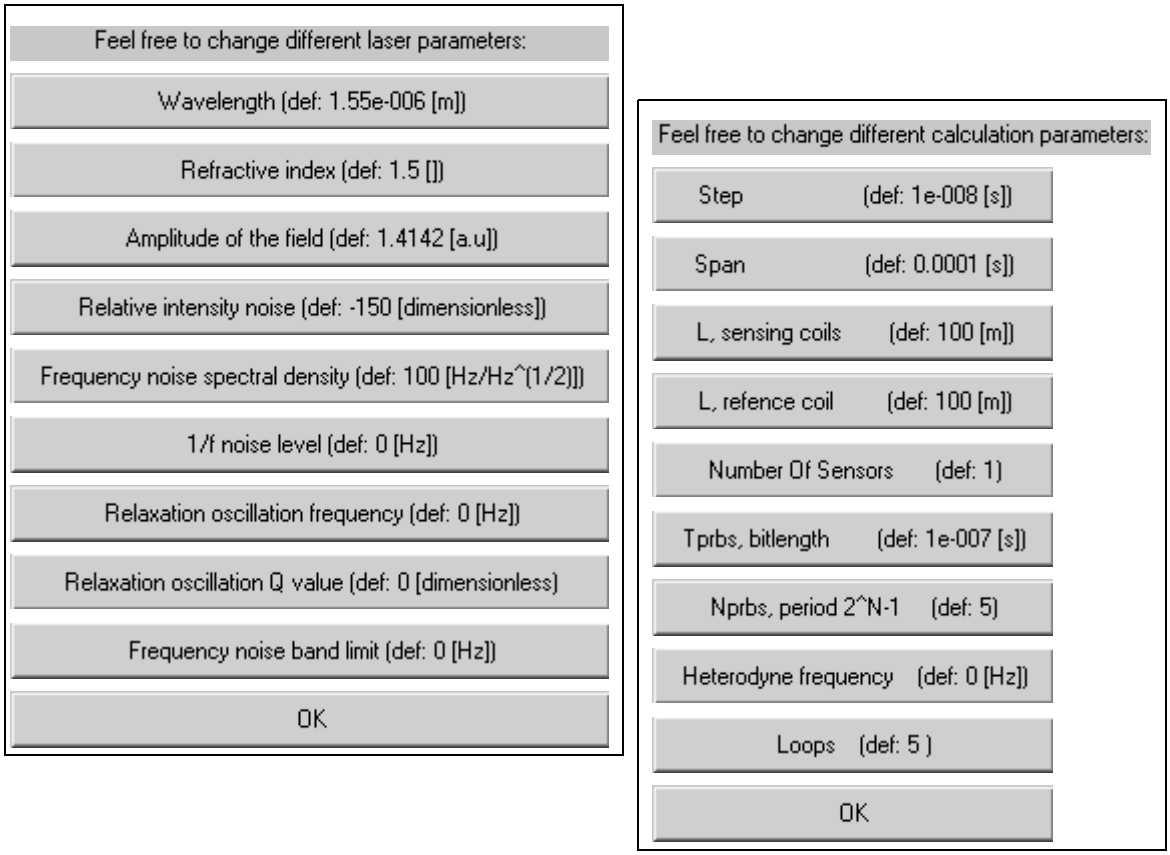

Figure 17 *User parameters in the program "coherentnetwork" used in the calculations*

noise, RIN, the frequency noise are given initially. The RIN is assumed to be white Gaussian noise and the user provides only the variance as an input. The frequency noise on the other hand can be adjusted in the frequency domain. It can be generated as white Gausssian noise, band limited, modified to include a harmonic resonance oscillation specified by an oscillation frequency and a Q-value or finally made to include 1/f noise specified by an edge frequency. The first user dialogue box includes these settings along with basic laser parameters. A second user dialogue box call for calculation parameters such as the calculation step and the span which have to be carefully chosen to account for effects appearing due to the frequency noise. The network is assumed to be on the form of network b in figure 15 and results valid for the single unbalanced interferometer are found at the first point when the parameter "Number of Sensors" is set to one. The length of the sensing coils, L, include the full length difference between two successive paths in the ladder and can not be individually adjusted. It is denoted

“L, sensing coil” (it is assumed that most of this length can be wound on a sensor coil used to pick up an external signal modulation). The parameter, “L, reference coil” is used to specify the path imbalance in the reference interferometer prior to the output port. Two parameters, “Tprbs, bitlength” and “Nprbs, period 2^N-1” are used to set the pseudo random binary sequence (PRBS) generator. The parameter “Heterodyne frequency” is used to shift the optical frequency of the field propagating in the first path of the network. This function is used only for the single path unbalanced interferometer case. An acousto-optic modulator is commonly employed to shift the optical frequency in one leg of the interferometer in order to generate a carrier frequency around which laser frequency modulation appears as sidebands. This is a method to measure the laser linewidth. It may also be used for the purpose of heterodyne demodulation of phase and frequency modulating signals. The “Loops” button is used to make the calculations a selected number of times with a given increment for any of the laser or network parameters. The full calculations are done for each value and the dependence of the selected parameter is visualized. Not appearing in the user interface are the input signal parameters. Harmonic signals can be applied both as a laser frequency modulation and as length modulations of the sensing coils.

In addition to the network output powers the program calculates the field power spectrum of the generated optical field and determines the linewidth.

7. Numerical results for a single unbalanced Mach-Zehnder interferometer

In this section some results from calculations are presented. The section is provided to describe, in general, how the laser source frequency noise transform into intensity noise by means of the unbalanced interferometer and how the field correlation properties determine the interferometer fringe visibility. The results rely on a proper choice of the step and span chosen for the calculations. Since the mechanisms involved in the coherent network can translate power in the frequency domain it is necessary to make sure that the step time is short enough. The step time may be thought of as the sampling period of an acquisition system connected to the detector. But, it is very important to understand that we are also trying to calculate the effects occurring in the optical domain by this sampling period. In reality, interference may result in power being shifted far up in the frequency domain when the coherence length of the optical field is shorter than the path length difference. Therefore we must carefully choose the

step time in order to assure that aliasing does not affect the result. A short step time is desired to make sure that aliasing is avoided. The first two following results will elucidate this issue.
Right through the calculations in this section we have used a steptime of 10 ns and a span of 1 ms. The span is limited by the computing power and will in turn limit the frequency resolution of the spectral results. The laser noise is simulated in the simplest possible way with the frequency noise and the RIN being white. The RIN is intentionally set to a low but realistic value, -150 dB/Hz, since it will not play an important role.
The results are presented in the form of resultsheets, containing input parameters and calculated spectra.

7.1 Changing the laser frequency noise spectral density

In our first example the laser frequency noise spectral density is varied from -20 dB to 60 dB $Hz/\sqrt{Hz}$ in five steps of 20 dB. The results are found in ***resultsheet A***. The program calculates the optical field properties and we present in the upper right diagram the optical power spectrum. As expected for white laser frequency noise the optical power spectrum follows a Lorentzian profile with a linewidth being dependent on the frequency noise spectral density. The calculated laser parameter table shows the obtained values for the coherence time and its related parameters, coherence length and optical field linewidth. The three first coherence times fall outside of a range in which the program can calculate the coherence time. Note, that this does not affect the network calculations in which the fields are correctly described. Again, this is just a limitation due to computing power. The two lowest laser frequency noise values would result in a very narrow linewidth field with no realistic counterpart. The linewidths obtained for 20, 40 and 60 dB $Hz/\sqrt{Hz}$ on the hand may be achieved in practice. Gas lasers, external cavity lasers and fiber lasers can have linewidths in the low kHz range and DFB semiconductor lasers typically in the range about 1-10 MHz.
Power spectra are calculated for the detected optical power. There is a risk for confusion between these spectra and the optical power spectrum. While the detected optical power shall be treated as the signal carrier being proportional to current and voltage in the receiver the optical power spectrum is applied to the optical field. The interferometer path length difference was set to 100 meters and adjusted to quadrature, i.e.where the undisturbed phase difference of the two fields on the output of the interferometer is $\pi/2$. The two topmost diagrams for the calculated network signals show the power spectral density in the full bandwidth of the calculation. The lower left diagram shows the power spectral density for resampled data to increase

the resolution at low frequencies. The lower right diagram shows the interferometer phase noise in the full bandwidth. As can be seen in the phase noise diagram the unbalanced interferometer has the effect of converting the white laser frequency noise into phase noise with predominance at low frequencies. The phase noise level falls of as a $sinc^2(f/f_0)$ function with $f_0=c/nl$. As long as the phase noise level is low the output intensity noise will follow this pattern. As seen, for the lowest setting of the laser frequency noise, -20 dB $Hz/\sqrt{Hz}$, the RIN noise floor appearing at -156 dB (since the average detected optical power is 1/2 of the input power) is reached above 1 MHz. The noise floor of the received power increase in proportion to the laser frequency noise and follow the phase noise pattern until a maximum at about -80 dB is reached. The noise pattern then changes and take on the shape of a Lorentzian function. Upon further increase of the laser frequency level the noise power will translate from lower to higher frequencies. The noise level in the low frequency regime will begin to fall with increasing laser frequency noise.

This behaviour can be understood by examining the interferometer phase noise. When the interferometer phase noise magnitude is far below a radian the output intensity is approximately a linear function of the interferometer phase. In contrast, when the phase noise magnitude is well above a radian the output intensity must be treated as a sinusoidal function of the interferometer phase. Hence, Bessel harmonics will develop and in effect move the spectral power to higher frequencies. This will also wipe away low frequency phase signals of amplitudes below 1 rad and is actually the mechanism involved in incoherent mixing. Phase signals cannot be detected simply because the phase noise power is higher than the signal power. Translated into the interferometer output intensity power spectrum it will appears as if the signals gradually disappears when the phase noise increase above the threshold which is found where the optical field coherence length coincides with the path length difference of the interferometer.

We show this effect in ***resultsheet B*** where we have used three laser frequency noise settings, -20, 20 and 60 dB $Hz/\sqrt{Hz}$. The signal was applied as a length modulation of one of the two interferometer paths. It had an amplitude of 2 μm and a frequency of 800 kHz. The phase signal distributes over several harmonics in the output power spectrum due to the interferometric non-linear conversion. As seen the signal disappears completely for the highest laser frequency noise level.

For the readers acquainted with heterodyne demodulation systems, in which an acousto-optic modulator is used to generate a carrier frequency within the detector bandwidth, it may be interesting to see the same series of simulated laser fields applied to such interferometers. These results are found in ***resultsheet C***. The above discussion holds also for this case but all features are centred around the carrier frequency, in this case 20 MHz. A feature not visualized in ***A*** is the centre frequency peak (customary denoted the monochromatic peak) dependence on the laser frequency noise. We can see that this peak disappears when the coherence length of the laser field drops below the path length difference of the interferometer. This is completely in accordance with theory and has the same explanation as that for low frequency signals above.

7.2 Changing the interferometer path length difference

The output noise frequency characteristics are certainly also dependent on the path length difference of the interferometer but in a different way. The results shown in ***resultsheet D*** are obtained with the path length difference of the interferometer set to 100, 316, 1000, 3160, 10000 m and with the white laser frequency noise at 40 dB $Hz/\sqrt{Hz}$. This laser frequency noise setting produces a coherence length of about 500 meters.

We notice first that the noise level again falls of like a $sinc^2(f/f_0)$ function with $f_0=c/nl$ but converts gradually to the Lorentzian shape when the path length difference is increased. The first dip in the noise function can be seen to move towards lower frequencies in accord with $f_0=c/nl$.

The low frequency noise, which is particularly important since it cover the sensor frequency band, increase in proportion to the path length difference until it reaches a maximum where it saturates. This can be seen in the resampled data shown in the lower left diagram.

The maximum at which the noise level saturates is determined by the optical frequency noise. When the path length difference is increased well above the coherence length of the laser the noise spectrum will rapidly approach that which would be obtained if two completely uncorrelated optical fields where mixed or if the path length difference was infinite. The output intensity noise power spectrum becomes fully determined by the laser noise properties.

Again the same conditions were applied to an interferometer incorporating an acousto optic modulator. The results are shown in ***resultsheet E***. We note that the spectral resolution hide the important details in a narrow frequency band around the carrier.

Finally, in ***resultsheet F*** are shown results with a signal applied to the interferometer as above. In this case the amplitude was set to 4 μm and the frequency to 90 kHz. Unlike when the fre-

quency noise is increased we cannot extinct the applied signals by increasing the path length difference. The reason for this may not be obvious but has got to do with the coherence time of the field, in this case more adequately denoted as the field decorrelation time. A phase modulating signal with frequency above the field decorrelation time will not disappear completely but instead behave very much as the monochromatic peak in a heterodyne system, i.e. it will transform into a smeared peak with Lorentzian shape. On the contrary, a signal of frequency well below the decorrelation time as was the case in the previous example in ***resultsheet B*** will disappear.

7.3 Final remarks on this section

In conclusion, we realize that the noise properties at the output of an interferometric network are critically dependent on the laser source noise properties. A network with more than one interference point will transform the laser frequency noise into output intensity noise in a complicated manner which will become difficult to follow by intuition. This section has provided a brief introduction to the features of coherent networks, knowledge which is useful when larger networks are analysed.

Resultsheets

chapter 7

Resultsheet A

Input parameters

lambda	1.55e-006	[m]
refractive index, n	1.5	
RIN	-150	[dB/Hz]
fNoise PSD	1.000000e-001	[Hz/Hz^(1/2)]
1/f fNoise	0	[Hz]
relax. osc. f.	0	[Hz]
relax. osc. Q.	0	
fNoise bandlimit	0	[Hz]
calc. option	Single Mach Zehnder configuration	
step	1e-008	[s]
span	0.001	[s]
nr of loops	5	
loop parameter	laserStruct.fNoisePSD	[Hz]
startvalue	0.1	
increment	20	[dB]
coil length, l	100	[m]
ref length, l	100	[m]
number of sensors	1	
AM modulation	n	
PRBSperiod, T	1e-007	[s]
shiftregister length, N	5	
FM modulation	n	
demodulation freq.	2e+007	[Hz]
signal ampl.	0	[m]
signal freq.	1e+009	[Hz]
demodulation freq.	2e+007	[Hz]

Calculated laser parameters

coherence time	coherence length	coherence length(fiber)	linewidth(3dB)
[s]	[m]	[m]	[kHz]
>1.023000e-005	>3069	>2046	<16
>1.023000e-005	>3069	>2046	<16
>1.023000e-005	>3069	>2046	<16
2.580000e-006	774	516	62
4.000000e-008	12	8	3979

Laser frequency noise and optical field power spectrum

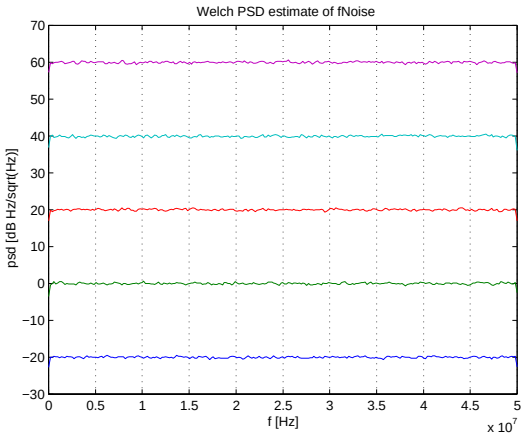

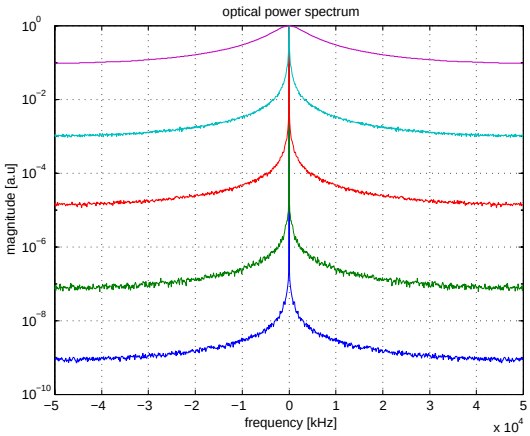

Calculated output intensity output power spectrum and phase noise power spectrum

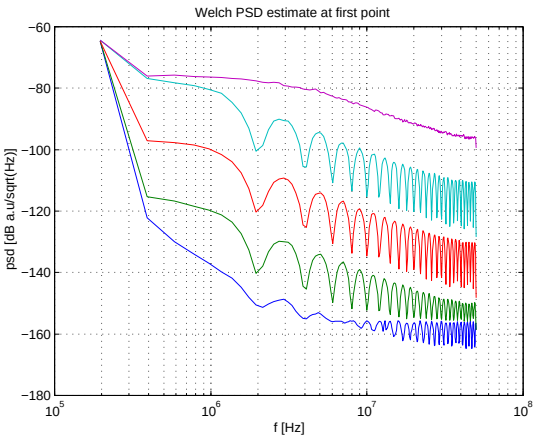

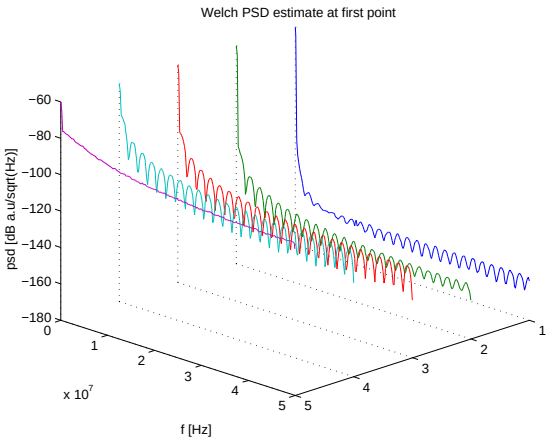

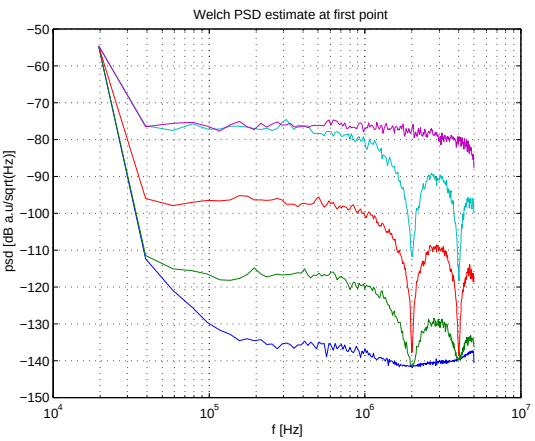

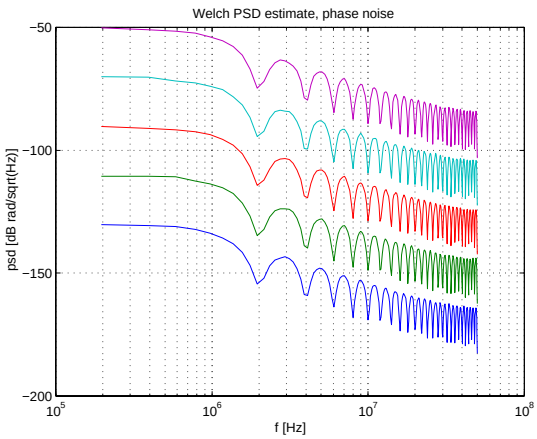

Resultsheet B

Input parameters

lambda	1.55e-006	[m]
refractive index, n	1.5	
RIN	-150	[dB/Hz]
fNoise PSD	1.000000e-001	[Hz/Hz^(1/2)]
1/f fNoise	0	[Hz]
relax. osc. f.	0	[Hz]
relax. osc. Q.	0	
fNoise bandlimit	0	[Hz]
calc. option	Single Mach Zehnder configuration	
step	1e-008	[s]
span	0.001	[s]
nr of loops	5	
loop parameter	laserStruct.fNoisePSD	[Hz]
startvalue	0.1	
increment	20	[dB]
coil length, l	100	[m]
ref length, l	100	[m]
number of sensors	1	
AM modulation	n	
PRBSperiod, T	1e-007	[s]
shiftregister length, N	5	
FM modulation	n	
demodulation freq.	2e+007	[Hz]
signal ampl.	0	[m]
signal freq.	1e+009	[Hz]
demodulation freq.	2e+007	[Hz]

Calculated laser parameters

coherence time	coherence length	coherence length(fiber)	linewidth(3dB)
[s]	[m]	[m]	[kHz]
>1.023000e-005	>3069	>2046	<16
>1.023000e-005	>3069	>2046	<16
>1.023000e-005	>3069	>2046	<16
2.580000e-006	774	516	62
4.000000e-008	12	8	3979

Laser frequency noise and optical field power spectrum

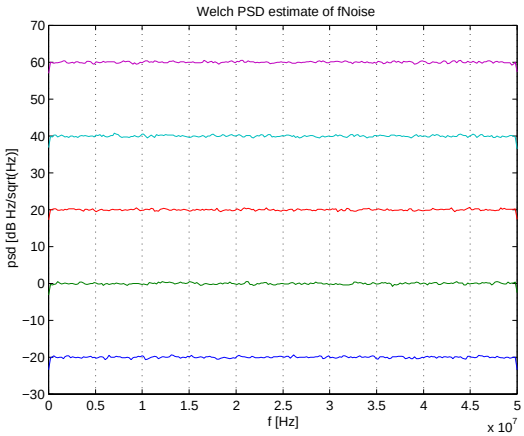

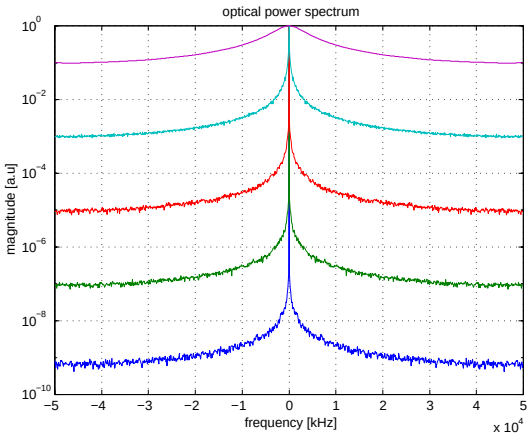

Calculated output intensity output power spectrum and phase noise power spectrum

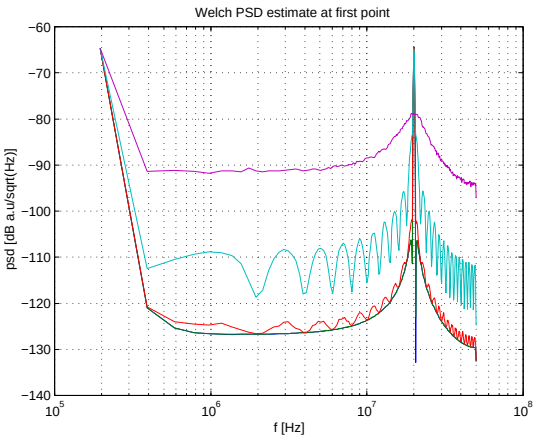

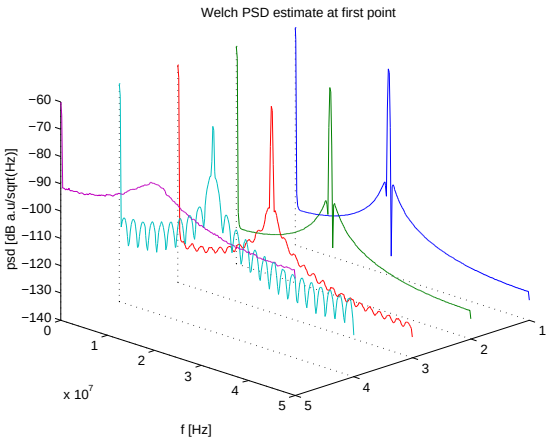

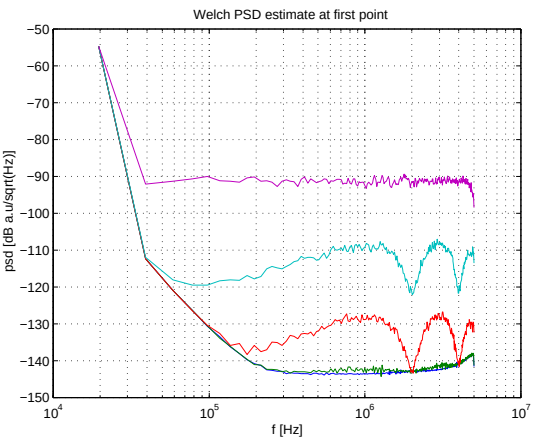

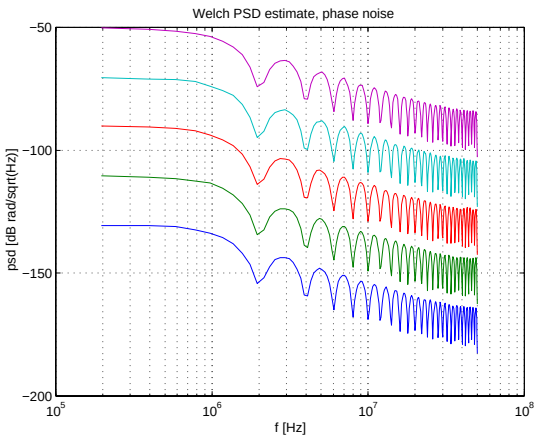

Resultsheet C

Input parameters

lambda	1.55e-006	[m]
refractive index, n	1.5	
RIN	-150	[dB/Hz]
fNoise PSD	1.000000e-001	[Hz/Hz^(1/2)]
1/f fNoise	0	[Hz]
relax. osc. f.	0	[Hz]
relax. osc. Q.	0	
fNoise bandlimit	0	[Hz]
calc. option	Single Mach Zehnder configuration	
step	1e-008	[s]
span	0.001	[s]
nr of loops	5	
loop parameter	laserStruct.fNoisePSD	[Hz]
startvalue	0.1	
increment	20	[dB]
coil length, l	100	[m]
ref length, l	100	[m]
number of sensors	1	
AM modulation	n	
PRBSperiod, T	1e-007	[s]
shiftregister length, N	5	
FM modulation	n	
demodulation freq.	2e+007	[Hz]
signal ampl.	0	[m]
signal freq.	1e+009	[Hz]
demodulation freq.	2e+007	[Hz]

Calculated laser parameters

coherence time	coherence length	coherence length(fiber)	linewidth(3dB)
[s]	[m]	[m]	[kHz]
2.680000e-006	804	536	59

Laser frequency noise and optical field power spectrum

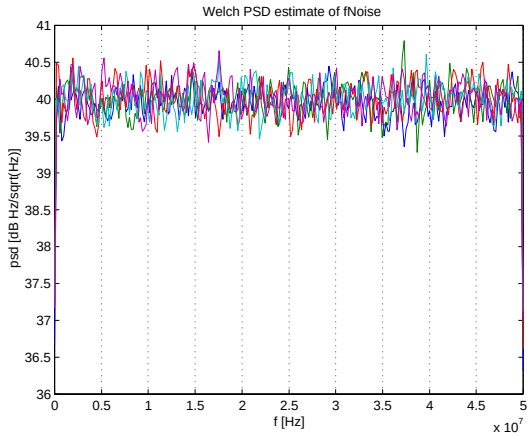

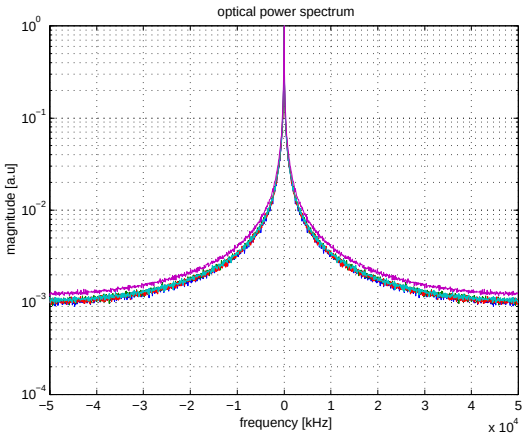

Calculated output intensity output power spectrum and phase noise power spectrum

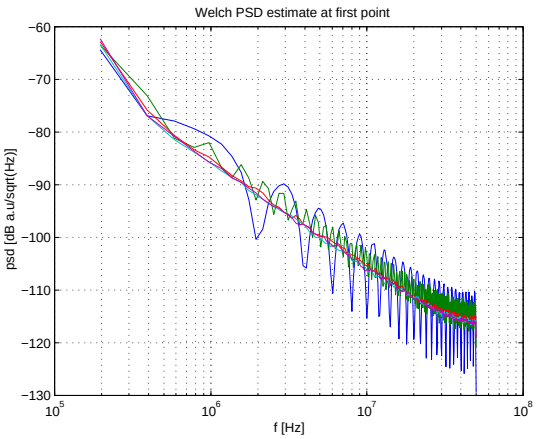

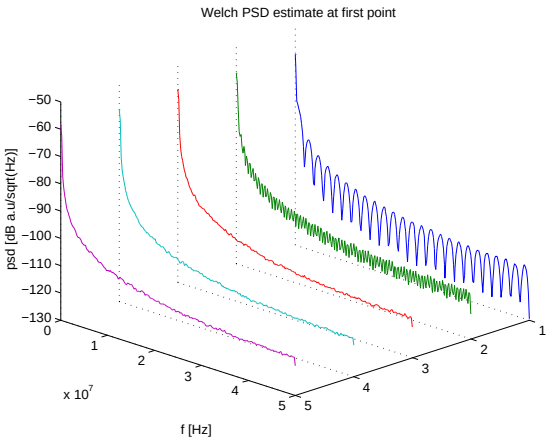

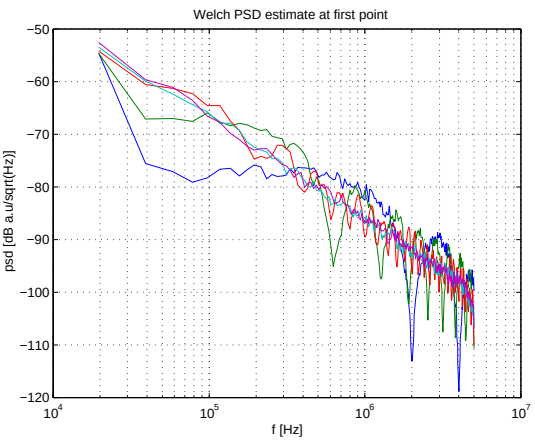

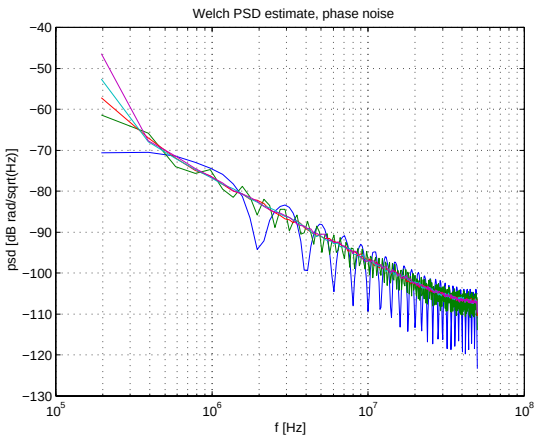

Resultsheet D

Input parameters

lambda	1.55e-006	[m]
refractive index, n	1.5	
RIN	-150	[dB/Hz]
fNoise PSD	1.000000e-001	[Hz/Hz^(1/2)]
1/f fNoise	0	[Hz]
relax. osc. f.	0	[Hz]
relax. osc. Q.	0	
fNoise bandlimit	0	[Hz]
calc. option	Single Mach Zehnder configuration	
step	1e-008	[s]
span	0.001	[s]
nr of loops	5	
loop parameter	laserStruct.fNoisePSD	[Hz]
startvalue	0.1	
increment	20	[dB]
coil length, l	100	[m]
ref length, l	100	[m]
number of sensors	1	
AM modulation	n	
PRBSperiod, T	1e-007	[s]
shiftregister length, N	5	
FM modulation	n	
demodulation freq.	2e+007	[Hz]
signal ampl.	0	[m]
signal freq.	1e+009	[Hz]
demodulation freq.	2e+007	[Hz]

Calculated laser parameters

coherence time	coherence length	coherence length(fiber)	linewidth(3dB)
[s]	[m]	[m]	[kHz]
2.750000e-006	825	550	58
2.880000e-006	864	576	55
2.340000e-006	702	468	68
2.380000e-006	714	476	67
2.990000e-006	897	598	53

Laser frequency noise and optical field power spectrum

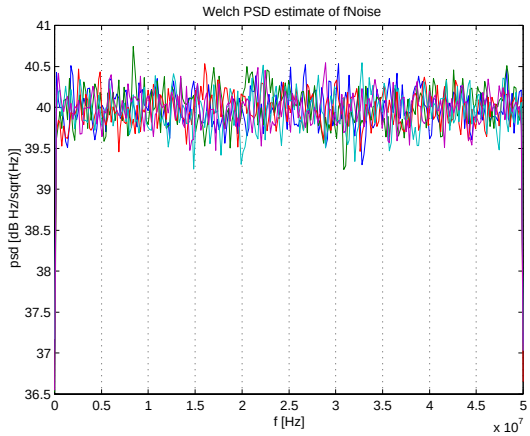

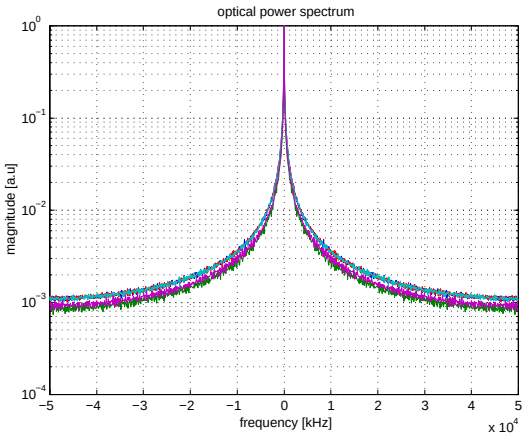

Calculated output intensity output power spectrum and phase noise power spectrum

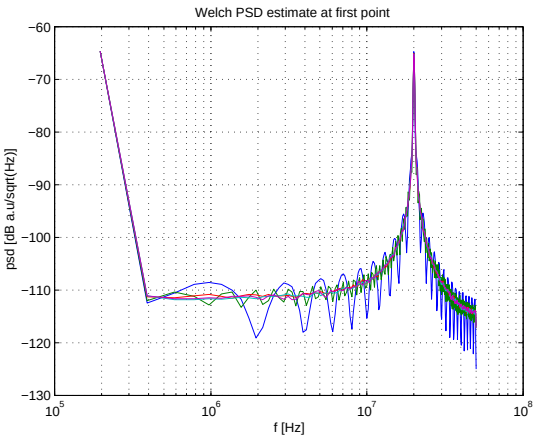

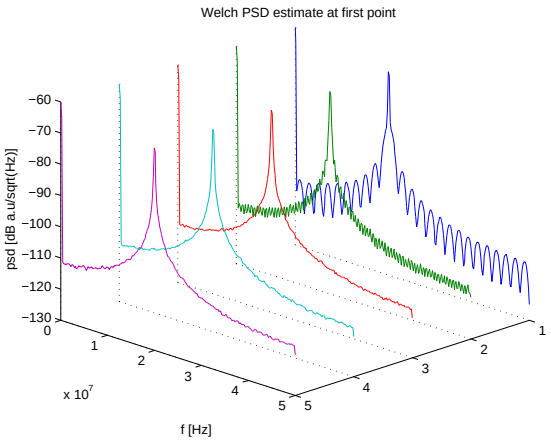

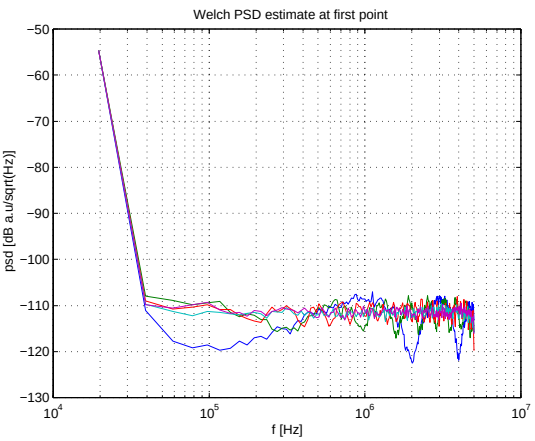

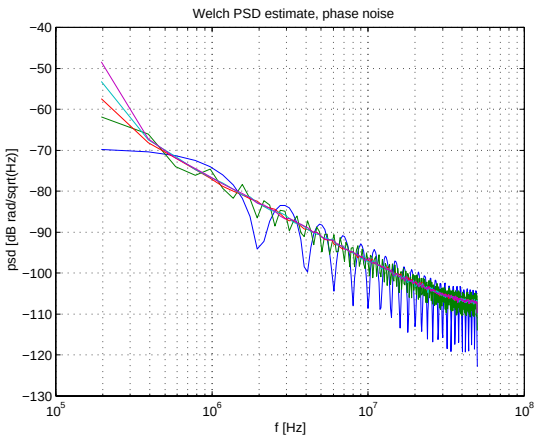

Resultsheet E

Input parameters

lambda	1.55e-006	[m]
refractive index, n	1.5	
RIN	-150	[dB/Hz]
fNoise PSD	1.000000e-001	[Hz/Hz^(1/2)]
1/f fNoise	0	[Hz]
relax. osc. f.	0	[Hz]
relax. osc. Q.	0	
fNoise bandlimit	0	[Hz]
calc. option	Single Mach Zehnder configuration	
step	1e-008	[s]
span	0.001	[s]
nr of loops	3	
loop parameter	laserStruct.fNoisePSD	[as is]
startvalue	0.1	[as is]
increment	40	[dB]
coil length, l	100	[m]
ref length, l	100	[m]
number of sensors	1	
AM modulation	n	
PRBSperiod, T	1e-007	[s]
shiftregister length, N	5	
FM modulation	n	
demodulation freq.	0	[Hz]
signal ampl.	2e-006	[m]
signal freq.	800000	[Hz]
demodulation freq.	0	[Hz]

Calculated laser parameters

coherence time	coherence length	coherence length(fiber)	linewidth(3dB)
[s]	[m]	[m]	[kHz]
>1.023000e-005	>3069	>2046	<16
>1.023000e-005	>3069	>2046	<16
4.000000e-008	12	8	3979

Laser frequency noise and optical field power spectrum

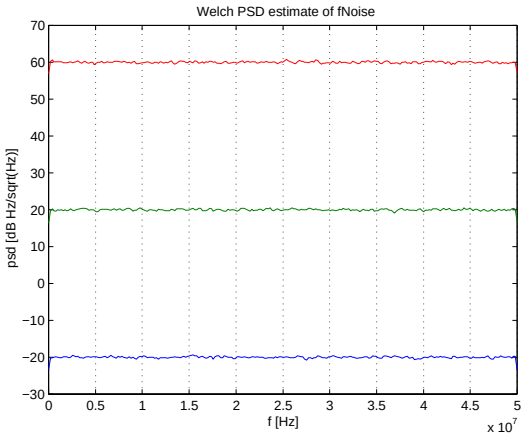

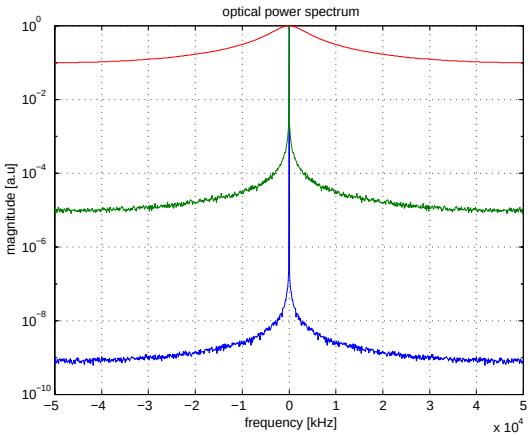

Calculated output intensity output power spectrum and phase noise power spectrum

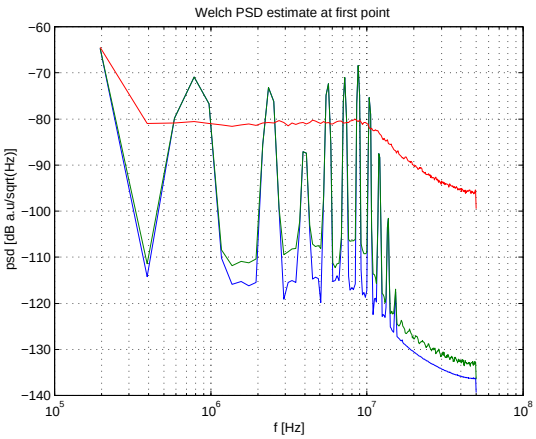

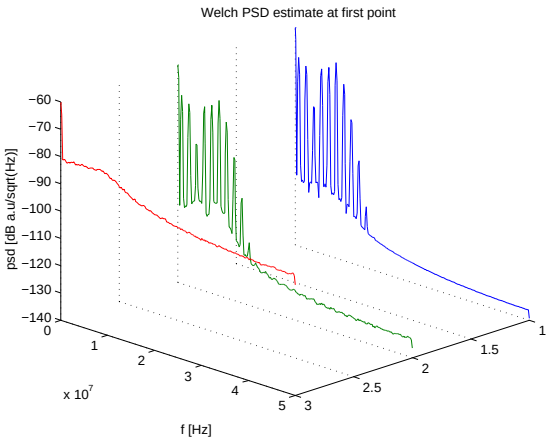

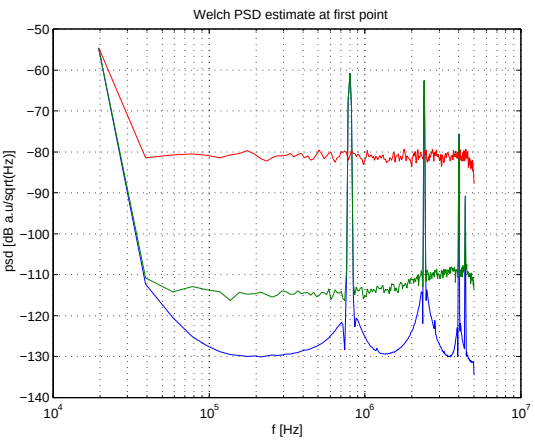

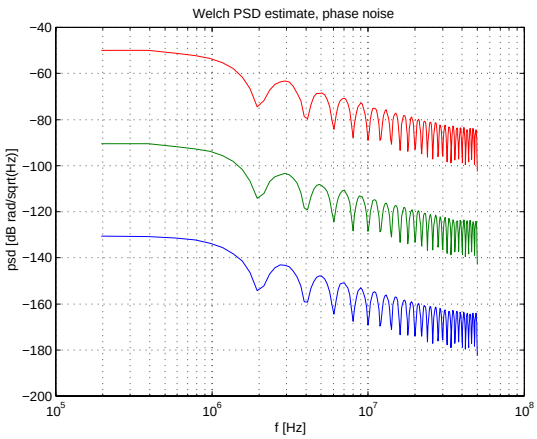

Resultsheet F

Input parameters

lambda	1.55e-006	[m]
refractive index, n	1.5	
RIN	-150	[dB/Hz]
fNoise PSD	100	[Hz/Hz^(1/2)]
1/f fNoise	0	[Hz]
relax. osc. f.	0	[Hz]
relax. osc. Q.	0	
fNoise bandlimit	0	[Hz]
calc. option	Single Mach Zehnder configuration	
step	1e-008	[s]
span	0.001	[s]
nr of loops	3	
loop parameter	networkStruct.l	[as is]
startvalue	100	[as is]
increment	20	[dB]
coil length, l	100	[m]
ref length, l	100	[m]
number of sensors	1	
AM modulation	n	
PRBSperiod, T	1e-007	[s]
shiftregister length, N	5	
FM modulation	n	
demodulation freq.	0	[Hz]
signal ampl.	4e-006	[m]
signal freq.	90000	[Hz]
demodulation freq.	0	[Hz]

Calculated laser parameters

coherence time	coherence length	coherence length(fiber)	linewidth(3dB)
[s]	[m]	[m]	[kHz]
2.390000e-006	717	478	67
3.100000e-006	930	620	51
2.510000e-006	753	502	63

Laser frequency noise and optical field power spectrum

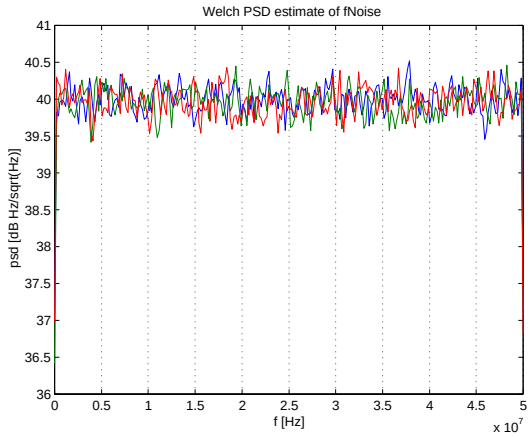

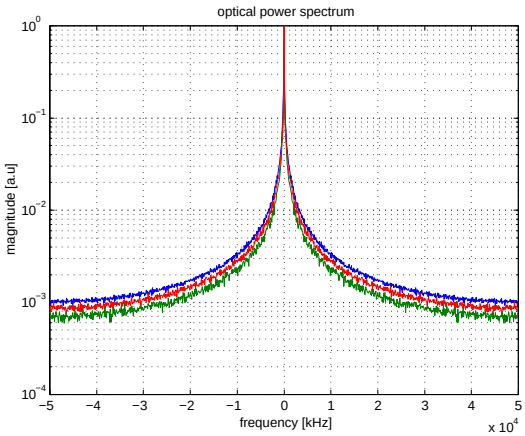

Calculated output intensity output power spectrum and phase noise power spectrum

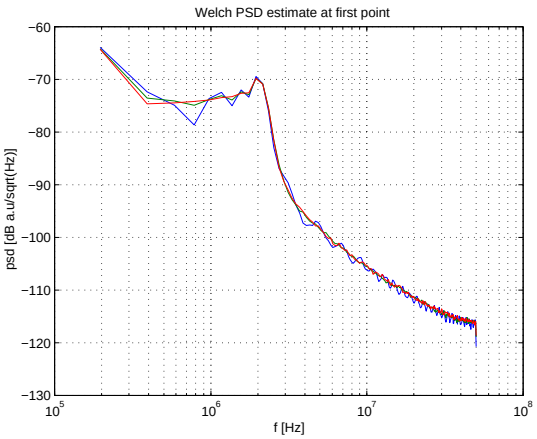

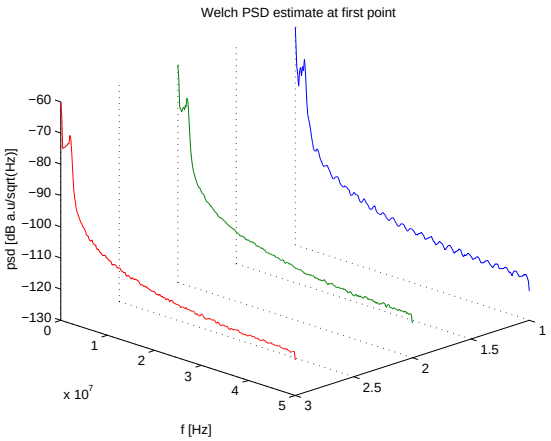

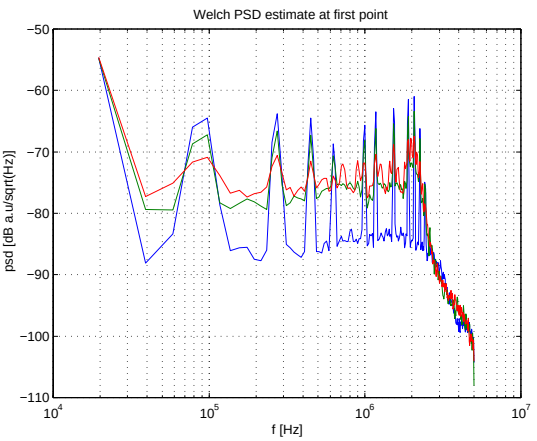

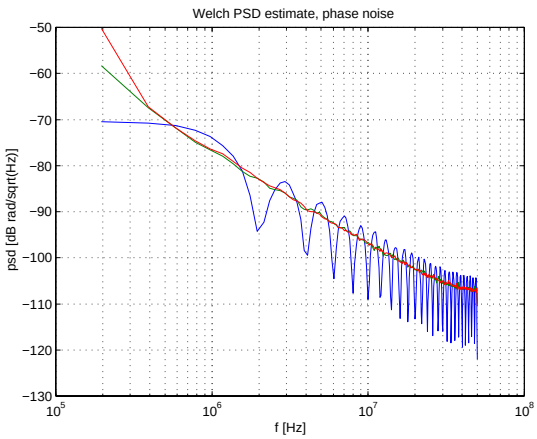

8. Numerical results for a nested interferometer network

Calculations based on equation (12) have been used to simulate the output power from various combinations of lasers and networks. As we shall see in the following results, crosstalk between sensors become a problem for a laser with narrow linewidth while the noise level in the demultiplexed signals become high for lasers with more broad linewidth. We have chosen to work with a five sensor nested network of the type shown in figure 15 to illustrate general tendencies. The calculations shown below were performed with a timestep (sampling interval) of 1 ns and a span of 0.3 ms. Hence, the frequency resolution is limited to 3.3 kHz. To enhance the resolution the span has to be increased. But the time step must be kept short to make sure that the high frequency content of the laser field is faithfully represented. For reasonable calculation times, the available computing power and the amount of calculations turned out to limit the span to about $3*10^5$ of the calculation step.

Two laser frequency noise levels at 20 and 60 dB $Hz/\sqrt{Hz}$ (10 and 1000 $Hz/\sqrt{Hz}$) are tested. The generated laser fields become comparable to what can be achieved in practice. The lower level yields a linewidth around 0.6 kHz which is narrow and represents a case which is approached by the best available sources suitable for this application, e.g. external cavity lasers and fiber lasers. The higher level yields a linewidth of 6 MHz which can be regarded as a quite typical value for DFB semiconductor lasers. The flat laser frequency noise spectrum is a fair approximation for semiconductor lasers whose relaxation oscillation resonance typically comes above 1 GHz while fiber lasers have their relaxation oscillation within the frequency range of interest, e.g between 100 and 1000 kHz. The path length difference between successive sensors and between the arms of the compensating interferometer was set to 40 m. The laser source has an output power of 1 (dimensionless), wavelength of 1.55 micrometer, RIN of *-150 dB/Hz.*

8.1 Passive network

In figure 18 is shown the calculated output power for a nested network. These result are for an unmodulated passive network. The phase noise that would arise in an interferometer with a 40 m path length difference is shown in the upper left diagram. The noise pattern follows the usual sinc functional behaviour and reaches its first minimum at 5 MHz (*c/nl*). The output intensity noise from the unmodulated network has a first minimum at 2.5 MHz which can be associated with a path length difference of *l=80 m*. The detailed pattern of the received spec-

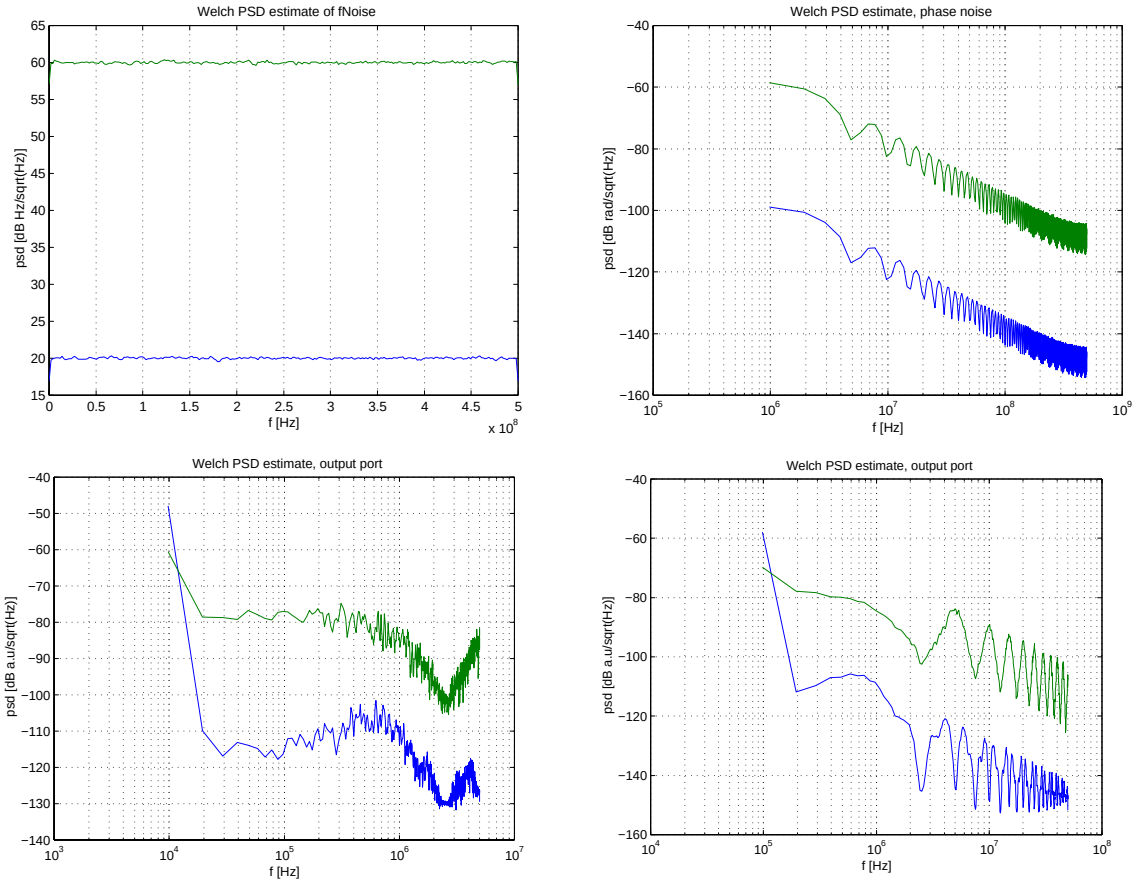

Figure 18 *A laser with the frequency noise characteristics (white noise) in the top left diagram applied to a 5 sensor nested network, l=40 m, produces an output intensity power spectrum shown in the bottom diagrams. For reference the top right diagram shows the phase noise that would be generated by a single unbalanced interferometer with l=40 m.*

trum is not easily predicted since it depends on the phase relationship between the mixed fields. Hence, the calculated spectra are not representative of all the outcomes of an experiment of this kind but rather represent one possible case. Anyway, the right hand spectrum shows that the noise power spectral density for the two tested fields differ by 40 dB at high frequencies in accordance with the laser frequency noise difference. For lower frequencies, as depicted in the left hand spectrum, the noise levels off and saturates at lower frequencies at a spectral density of about -80 dB $1/\sqrt{Hz}$. If the laser frequency noise is further increased the spectrum will gradually turn into a Lorentzian function as was explained in chapter 7.

8.2 PRBS amplitude modulated light applied to the network

When the laser intensity is modulated by a PRBS sequence the output intensity power spectrum turns into a combination of the passive network spectrum and the PRBS spectrum. We show in figure 19 the resulting spectrum obtained when the 31 bit length (n=5) PRBS code

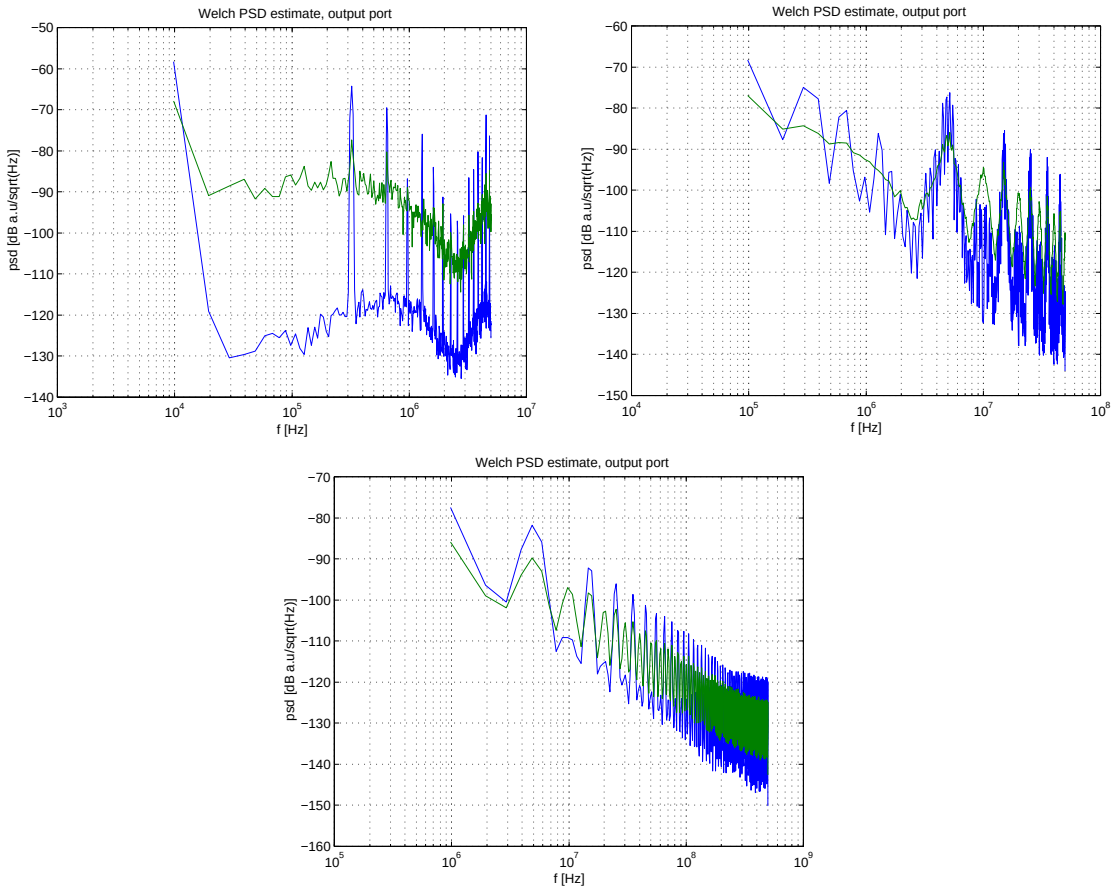

Figure 19 *Calculated spectrum with the laser intensity modulated by a 31 bit PRBS (n=5). Re-sampling was used to increase the spectral resolution in the lower frequency range (The reason for three diagrams).*

was used. The PRBS spectral features are found overlaid the passive network spectrum for the high coherence case. The first frequency peak appears at 320 kHz corresponding to the cycle repetition rate of the PRBS. For the laser field with high frequency noise (low coherence) it is seen that the PRBS peaks are suppressed and almost not discernible.

8.3 Applied signal on one of five sensor coils

A phase signal with a frequency of 15 kHz was applied to the first of five sensor coils. As seen in the left hand diagram the baseband signal is almost completely hidden in noise for the high laser frequency noise case while it is clearly visible for the low laser frequency noise case. Expectably, the ground tone and a series of Bessel harmonics arise as a result of the nonlinear interferometric conversion of the phase signal. Since several two-beam interferometers contribute to the signal the total signal amplitude may very well be higher than expected for one interferometer as is the case here. For the 60 dB $Hz/\sqrt{Hz}$ laser frequency noise level a single

interferometric signal is expected, i.e the one arising as a result of the balanced interferometer formed by the two shortest paths in the network and the compensating interferometer. This signal can not be discerned in the noise arising in the network.

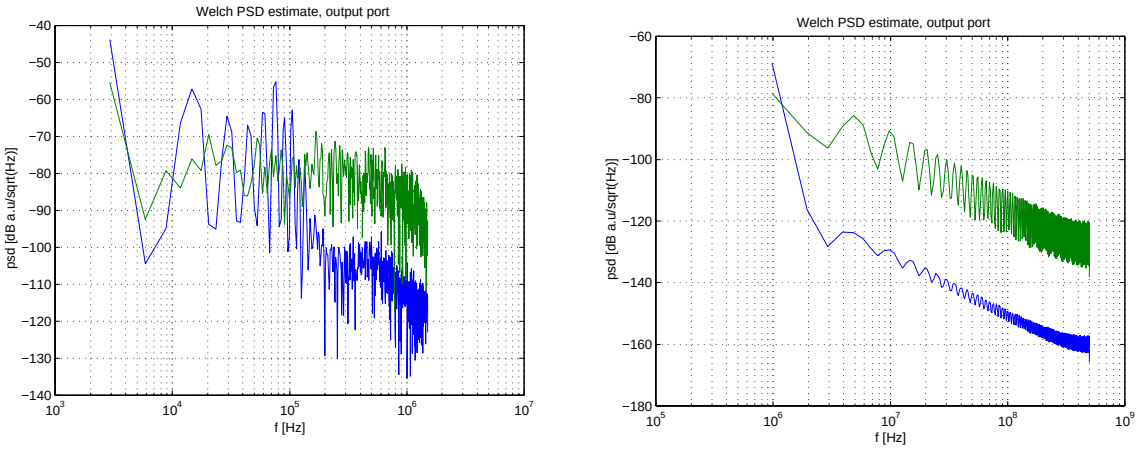

Figure 20 *Calculated spectrum with a sinusoidal signal applied as a length modulation of the first coil. The signal amplitude was 1 mm and the frequency was 15 kHz.*

8.4 Applied signal and PRBS amplitude modulation

When the PRBS modulation is applied to the network carrier tones beginning from 320 kHz appears. A certain fraction of the baseband signal is shifted upwards in the frequency domain and appears as sidebands around the PRBS carriers. According to our earlier discussion, the baseband signal does not disappear since a DC component of the optical carrier always remains. The right hand diagram, displaying the spectral features all the way up to the Nyquist frequency of the calculations, is shown just to confirm that the spectral power is on its way

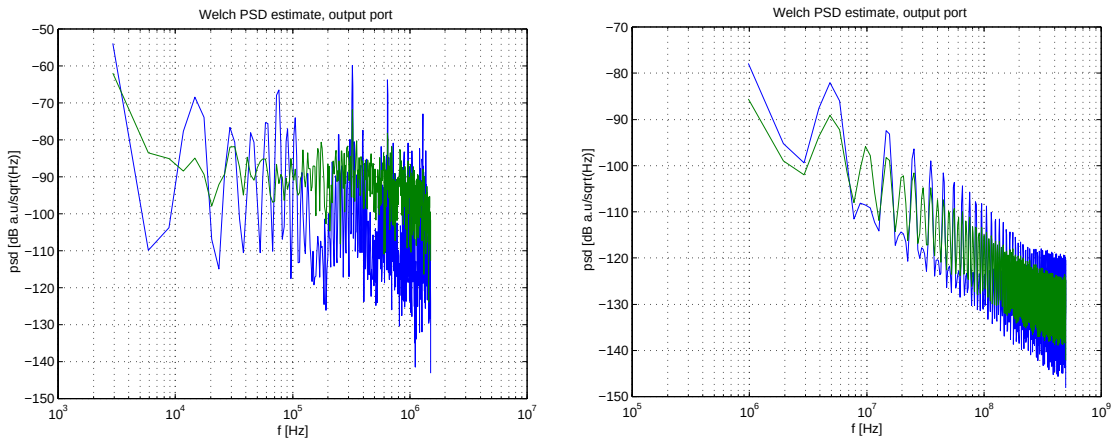

Figure 21 *Calculated spectrum with PRBS and a sinusoidal signal applied as a length modulation of the first coil. The signal amplitude was 1 mm and the frequency was 15 kHz.*

down. Since the calculations involve operations which may move the signal power up in the frequency domain it is important to make sure that aliasing does not occur. The higher the laser frequency noise and the longer the path length differences are in the network the more power is shifted towards higher frequencies. Eventually when either the laser frequency noise or the network path length differences are increased, it becomes necessary to decrease the calculation step further.

8.4.1 Demultiplexed signal

Demultiplexing is simulated by multiplication of the calculated output intensity signal with a bipolar reference PRBS (switching between levels of 1 and -1). In a practical system, a low pass filter shall be used to reject the high frequency components of the demultiplexed signals. The diagrams shown in figure 22 for the low laser frequency noise case of 20 dB $Hz/\sqrt{Hz}$ depict the signals prior to this filtering. Consequently, the PRBS carriers are still present. However, the important result appears in the baseband. Six reference PRBS are multiplied to the output intensity signal and their phase and time delay were set to be synchronized with the carriers in the network. The sensor signal applied at coil 1 is expected to appear at channel 1 and the signal appearing on the other channel would be ideally zero. As we can see the signal is visible on all channels which we attribute with the cross-correlation between the involved optical fields. The signal level is found to decrease with increasing channel order but is still appreciable for all channels. In view of the correlation properties of the network the higher level for channel 1 must also be considered as being the result of several correlation components superimposed to form the net output. Thus, the desired signal constitutes only a fractional part of the

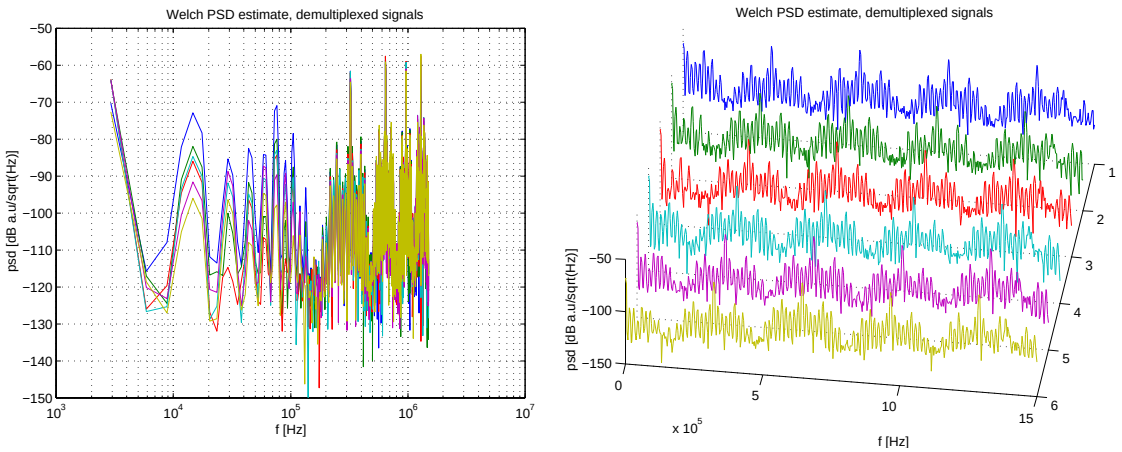

Figure 22 *Demultiplexed signals for the low laser frequency noise case of 20 dB* $Hz/\sqrt{Hz}$.

obtained signal level. Without further examination of this result we shall simply conclude that CDM does not work as desired under these conditions.

The results obtained with the 60 dB $Hz/\sqrt{Hz}$ level of laser frequency noise are shown in the two top diagrams of figure 23. The signal is now hardly visible and we note that if it is present

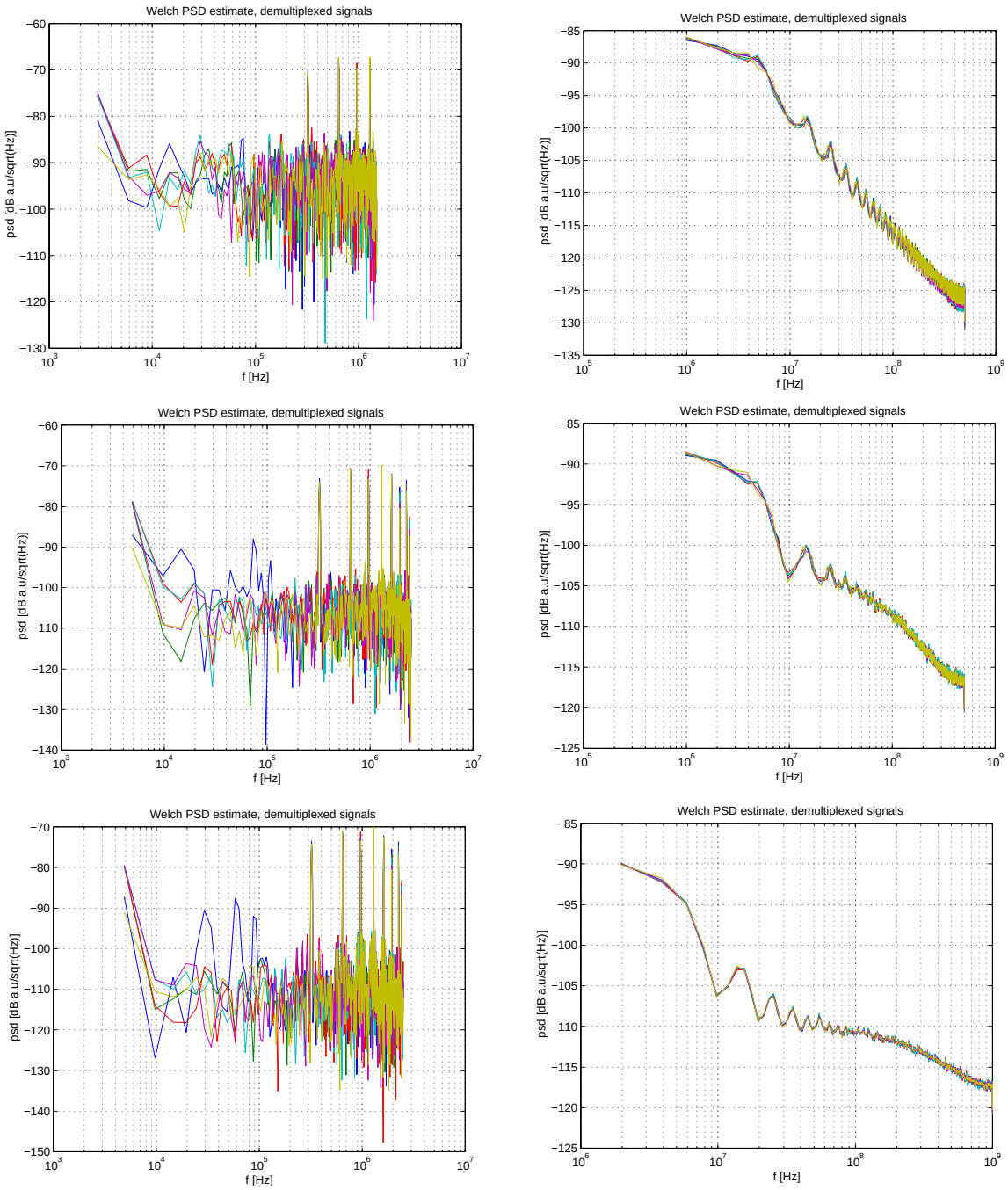

Figure 23 *Demultiplexed signals with a laser frequency noise of 1000 (60 dB) $Hz/\sqrt{Hz}$ in the top diagrams, 5000 (74 dB) $Hz/\sqrt{Hz}$ in the middle diagrams and with 10000 (80 dB) $Hz/\sqrt{Hz}$ in the bottom diagrams.*

its amplitude is much lower than above. The noise in the baseband becomes much higher for this case. Since the resolution is poor it is hard to estimate the signal condition at channel 1. But, clearly, the conditions are worse than in the case of a signal applied to a passive network with the 0.6 kHz linewidth laser while they might be better than for the case with a 6 MHz linewidth laser (figure 20). Even though the noise level is comparably high, a slight hope for the multiplexing method may be obtained by noting that the signal does not seem to appear at the other channels. The noise at the other channels produce spectral power of a magnitude comparable with the power in channel one and it is fair to assume that the noise power on the average is approximately the same also in channel 1. Hence, the signal-to-noise ratio in channel 1 is far from that desired and it is necessary to decrease the noise power. The only remaining way to decrease the noise power in the baseband is, which may seem contradictory, to increase the laser frequency noise level in order to decrease the laser field coherence time (length).

It is possible to increase the laser frequency noise by another factor of 10 from 1000 (60 dB) to 10000 $Hz/\sqrt{Hz}$ before aliasing becomes a problem. The results for 5000 $Hz/\sqrt{Hz}$ and 10000 $Hz/\sqrt{Hz}$ are also shown in figure 23 where we can see that the baseband noise floor in the demultiplexed channels decreases and that the signal can now be discerned at channel 1 while it does not appear on the other output channels. The right hand diagrams show the full spectrum of the calculated output intensity. The bump below 100 MHz shall be associated with the PRBS harmonics and the power at higher frequencies with laser frequency noise being transposed by the network. We note the output intensity noise frequency band is approaching the bandwidth of the calculation. Further increase of the laser frequency noise require that we decrease the calculation step (sampling period) even further to assure that the results are correct. Unfortunately the spectral resolution decrease proportionally since we must decrease the time span. The following result for a laser frequency noise at 10000 $Hz/\sqrt{Hz}$ is obtained with a calculation step of 0.1 ns and a time span of 30 μs.We can no longer resolve the signal and we conclude that calculations with this step time are not being meaningful with the current program code and the available computing speed. But the general tendency was shown already in figure 23 and we are ready to draw some conclusions from these results.

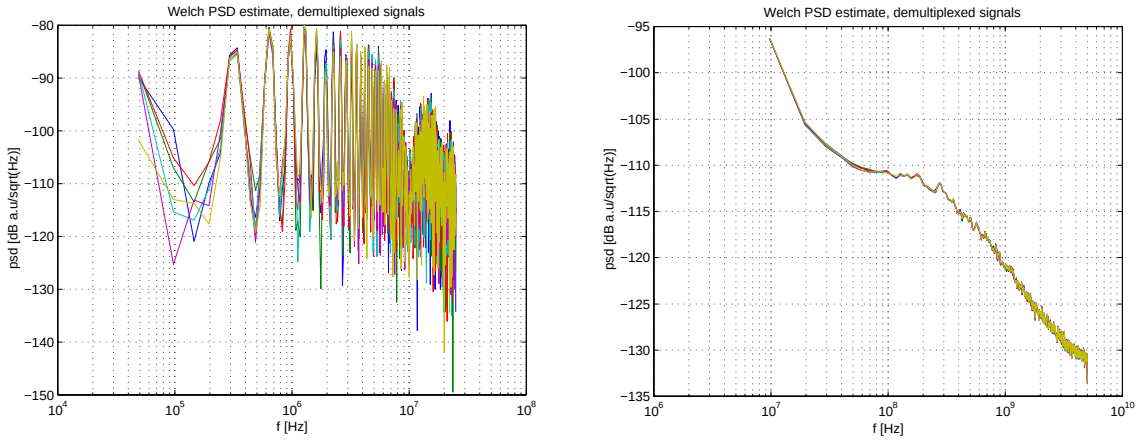

Figure 24 *Demultiplexed signals with a laser frequency noise of 10000 (80 dB)* $Hz/\sqrt{Hz}$. *Calculation time step set 0.1 ns and span set to 30* μs.

9. Conclusions

We have explored CDM for optical fiber sensor networks in several steps beginning with the detailed code properties giving rise to crosstalk. Most of these properties can be associated with the non-ideal characteristics in the electronic circuits used to implement CDM. Even though careful electronic design is required it has been found possible to construct low cross-talk systems with sensor-to-sensor crosstalk levels beneath a level of -60 dB, partly based on previous practical experience [5]. This level of crosstalk is probably going to be more than sufficient for many applications. Particularly, if the elements are working in groups defining antennas in the field to be measured, e.g. acoustic.

We demonstrated the ideal behaviour of a network of intensity modulating devices multiplexed with CDM just in order to show that no fundamental limit is present in this case.

On the other hand, interferometric networks incorporating phase sensitive devices, generally suffer from cross mixing products and phase noise leading to enhanced sensor to sensor cross-talk and a reduced signal-to-noise ratio. The main task of this work was to find out if CDM could be made to work satisfactory in interferometric networks.

In order to reach this goal it was necessary to take on a rather basic statistical approach with numerical calculations describing how the laser frequency noise transforms into output intensity noise and how the network parameters determine the field mixing properties. Chapter 7 was included to provide general insight into this area. The output of a single unbalanced inter-

ferometer was simulated for various parameter settings and the dependence of the laser frequency noise and of the interferometer path length difference were elucidated.

Our numerical results for the CDM nested network shows that a low coherence laser is required to avoid crosstalk between sensors. We saw in figure 22 that the signal from one network sensing coil appears at all the output channels even though ideal PRBS properties were used in the calculations. It was concluded that crosstalk arise due to the appearance of mixing products as described in section 4.1.5 and we do not see any other possibility to circumvent this problem than to use a low coherence laser if CDM is the multiplexing method.

Unfortunately, a low coherence laser is generally a laser with a comparably high laser frequency noise level. Consequently, it will generate more output noise in interferometric networks. The most obvious problem is that careful balancing is required to suppress the noise generated when fields having experienced approximately equal delay are mixed. Throughout the calculations we have assumed ideal conditions with perfect balancing and this noise is not seen. In practice, a precision better than 1 cm will be hard to achieve and noise caused by this imbalance will develop. It can be quite easily predicted using the relation

$$\Delta\phi = \frac{2\pi nl}{c_0}\Delta\nu \tag{16}$$

between the interferometer phase deviations and the laser frequency deviations valid for phase deviations well below *1 rad*. We find that the laser frequency noise levels of 20, 60 and 80 dB $Hz/\sqrt{Hz}$ give rise to phase noise levels of -170, -130 and -110 dB $rad/\sqrt{Hz}$ respectively assumed that the residual path imbalance is 1 cm. Typically, for these kind of systems the required resolution lies at about -120 dB $rad/\sqrt{Hz}$ and we see that this level is exceeded for the last case. Hence, lasers with even higher frequency noise levels may not be useful.

But for this case we must compare this noise term with the noise generated by the network as predicted by the calculation. In figure 23 the demultiplexed signals at the output of the network were shown. The noise levels in the sensor frequency band are not accurately reproduced due to the limited calculation bandwidth but we approximate the levels to -95, -105 and -115 dB $1/\sqrt{Hz}$. These levels are normalized to the network input power and we need to relate them to the power level corresponding to a *1 rad* phase deviation. Each nested interferometer in the simulated five sensor network will produce a mean detected optical power of a fraction of 1/72

of the input power. Thereby, it is easily found that the noise levels normalized to the input optical power relate to an equivalent phase noise level by the relation

$$\Delta\phi = 72\Delta P \tag{17}$$

where ΔP is the detected optical noise power. We arrive at equivalent phase noise levels of -48, -58 and -68 dB $rad/\sqrt{Hz}$ corresponding to the noise levels in figure 23. Thus, the developed noise is far above the required resolution at -120 dB $rad/\sqrt{Hz}$ and will be the dominating noise source for a well balanced system. These results were obtained for a five sensor network and we can expect an increased phase noise level with an increased number of sensors. The required resolution originates in the achievable sensitivity of the applied sensors. The resolution of -120 dB $rad/\sqrt{Hz}$ can be traced to the required acoustic sensitivity for hydrophone systems capable of resolving acoustic signals down to the ambient acoustic noise floor. It may become possible to construct sensing coils with enhanced sensitivity relieving the required resolution but to the cost of the dynamic range which is typically limited in the other end to signal amplitudes of about *1 rad* depending on choice of demodulation technique. In such a case CDM may prove to be a useful method. Nonetheless we judge that other multiplexing methods, not entailing fundamental detection limits, are preferable.

9.1 Concluding remarks

Although CDM has been shown previously to be a useful multiplexing method in optical fiber sensor networks due to its low optical power requirement, it seems as if it is less useful than other methods in high resolution interferometer systems due to its inability to extract cross correlation terms arising in networks of this kind. A possible way to circumvent this problem is to use broad linewidth, low coherence laser sources. However, to the cost of an increased noise floor in the frequency band of interest since no known laser source has got both broad linewidth and a relatively low level of frequency noise in the frequency band ranging up to about 100 kHz.

10. References

[1] H. S. Al-Raweshidy and D. Uttamchandani, “Spread spectrum technique for passive multiplexing of interferometric optical fiber sensors,” Optics Communications 80(1), 18-22 (1990).

[2] S. H. Poland, J. P. Bengtsson, M. Bhatnagar, K. C. Ravikumar, M. J. de Vries, and R. O. Claus, “Multi-Measurand Multiplexed Extrinsic Fabry-Perot Interferometric Sensors,” Proceedings of Smart Structures and Materials: Smart Sensing, Processing and Instrumentation 2191, 58-66 (1994).

[3] A. D. Kersey, “Distributed and multiplexed fiber optic sensors,” in Fiber Optic Sensors: An Introduction for Engineers and Scientists, E. Udd, Ed. New York: John Wiley & Sons, Inc., 1991, pp. 325-368.

[4] A. D. Kersey, A. Dandridge, and M. A. Davis, “Low-crosstalk code division multiplexed interferometric array,” Electronics Letters, vol. 28, pp. 351-352, 1992.

[5] F. Kullander, C. Laurent, S. Zyra, and H. Geis, “Crosstalk reduction in a code division multiplexed optical fiber sensor system,” Optical engineering, vol. 37, pp. 2104-2107, 1998.

[6] F. Kullander, “A Novel Algorithm for Passive Demodulation of Optical Fiber Interferometric Signals Using a 3x3 Coupler”, presented at OFS 2000, SPIE vol. 4185, pp 480-483.

[7] Y. Weissman, Optical network theory. Norwood: Artech House, Inc., 1992.

[8] L. A. Coldren and S. W. Corzine, Diode lasers and photonic integrated circuits. New York: John Wiley & Sons, Inc., 1995.

[9] J. W. Goodman, Statistical optics. New York: John Wiley & Sons, Inc., 1985.

[10] F. Kullander, B. Knuthammar, “Fiber laser hydrophones, an introductory survey”, User report no. FOA-R--00-01779-409--SE, Dec. 2000.